U.S. Department of Transportation

Federal Railroad Administration

Predicting Fully-Developed Passenger Rail Car Fire Heat Release Rate

Office of Research,
Development
and Technology
Washington, DC 20590

DOT/FRA/ORD-20/32

Final Report
August 2020

REPORT DOCUMENTATION PAGE

Form Approved

OMB No. 0704-0188

1. AGENCY USE ONLY (Leave blank)	2. REPORT DATE	3. REPORT TYPE AND DATES COVERED
	August 2020	Technical Report September 2018–September 2019

4. TITLE AND SUBTITLE

Predicting Fully-Developed Passenger Rail Car Fire Heat Release Rate

5. FUNDING NUMBERS

693JJ618C000022

6. AUTHOR(S)

Fengchang Yang, Jonathan Hodges, Christian Rippe, Stefan Kraft, and Brian Lattimer

7. PERFORMING ORGANIZATION NAME(S) AND ADDRESS(ES)

Jensen Hughes, Inc.
3610 Commerce Drive, Suite 817
Baltimore, MD 21227

8. PERFORMING ORGANIZATION REPORT NUMBER

9. SPONSORING/MONITORING AGENCY NAME(S) AND ADDRESS(ES)

U.S. Department of Transportation
Federal Railroad Administration
Office of Railroad Policy and Development
Office of Research, Development and Transportation
Washington, DC 20590

10. SPONSORING/MONITORING AGENCY REPORT NUMBER

DOT/FRA/ORD-20/32

11. SUPPLEMENTARY NOTES

COR: Melissa Shurland

12a. DISTRIBUTION/AVAILABILITY STATEMENT

This document is available to the public through the FRA website.

12b. DISTRIBUTION CODE

13. ABSTRACT (Maximum 200 words)

This report provides the results of the initial development of scaling laws for use in developing cost effective experimental measurements of a passenger rail car heat release rate (HRR) history as well as modeling approaches for predicting passenger rail car HRR. Scaling laws were successfully developed to predict the fire dynamics and material burning behavior in pre-flashover and fully-developed fires. In addition, a finite element (FE) model for window failure was developed to support the design of small scale windows. Fire Dynamics Simulator (FDS) was used to provide detailed predictions of the fire HRR history using a pyrolysis model for material burning. In addition, a simplified model was created for use by designers and operators. Future work is recommended to generate data to further validate the scaling laws and models.

14. SUBJECT TERMS

Rail car, heat release rate, HRR, heat release rate per unit area, HRRPUA, scaling law, fully-developed fire, window failing, fire dynamics simulator, FDS, rolling stock, passenger rail

15. NUMBER OF PAGES

76

16. PRICE CODE

17. SECURITY CLASSIFICATION OF REPORT	18. SECURITY CLASSIFICATION OF THIS PAGE	19. SECURITY CLASSIFICATION OF ABSTRACT	20. LIMITATION OF ABSTRACT
Unclassified	Unclassified	Unclassified	

NSN 7540-01-280-5500

Standard Form 298 (Rev. 2-89)

Prescribed by ANSI
Std. 239-18
298-102

METRIC/ENGLISH CONVERSION FACTORS

ENGLISH TO METRIC	METRIC TO ENGLISH
LENGTH (APPROXIMATE)	**LENGTH (APPROXIMATE)**
1 inch (in) = 2.5 centimeters (cm)	1 millimeter (mm) = 0.04 inch (in)
1 foot (ft) = 30 centimeters (cm)	1 centimeter (cm) = 0.4 inch (in)
1 yard (yd) = 0.9 meter (m)	1 meter (m) = 3.3 feet (ft)
1 mile (mi) = 1.6 kilometers (km)	1 meter (m) = 1.1 yards (yd)
	1 kilometer (km) = 0.6 mile (mi)
AREA (APPROXIMATE)	**AREA (APPROXIMATE)**
1 square inch (sq in, in^2) = 6.5 square centimeters (cm^2)	1 square centimeter (cm^2) = 0.16 square inch (sq in, in^2)
1 square foot (sq ft, ft^2) = 0.09 square meter (m^2)	1 square meter (m^2) = 1.2 square yards (sq yd, yd^2)
1 square yard (sq yd, yd^2) = 0.8 square meter (m^2)	1 square kilometer (km^2) = 0.4 square mile (sq mi, mi^2)
1 square mile (sq mi, mi^2) = 2.6 square kilometers (km^2)	10,000 square meters (m^2) = 1 hectare (ha) = 2.5 acres
1 acre = 0.4 hectare (he) = 4,000 square meters (m^2)	
MASS - WEIGHT (APPROXIMATE)	**MASS - WEIGHT (APPROXIMATE)**
1 ounce (oz) = 28 grams (gm)	1 gram (gm) = 0.036 ounce (oz)
1 pound (lb) = 0.45 kilogram (kg)	1 kilogram (kg) = 2.2 pounds (lb)
1 short ton = 2,000 pounds (lb) = 0.9 tonne (t)	1 tonne (t) = 1,000 kilograms (kg) = 1.1 short tons
VOLUME (APPROXIMATE)	**VOLUME (APPROXIMATE)**
1 teaspoon (tsp) = 5 milliliters (ml)	1 milliliter (ml) = 0.03 fluid ounce (fl oz)
1 tablespoon (tbsp) = 15 milliliters (ml)	1 liter (l) = 2.1 pints (pt)
1 fluid ounce (fl oz) = 30 milliliters (ml)	1 liter (l) = 1.06 quarts (qt)
1 cup (c) = 0.24 liter (l)	1 liter (l) = 0.26 gallon (gal)
1 pint (pt) = 0.47 liter (l)	
1 quart (qt) = 0.96 liter (l)	
1 gallon (gal) = 3.8 liters (l)	
1 cubic foot (cu ft, ft^3) = 0.03 cubic meter (m^3)	1 cubic meter (m^3) = 36 cubic feet (cu ft, ft^3)
1 cubic yard (cu yd, yd^3) = 0.76 cubic meter (m^3)	1 cubic meter (m^3) = 1.3 cubic yards (cu yd, yd^3)
TEMPERATURE (EXACT)	**TEMPERATURE (EXACT)**
[(x-32)(5/9)] °F = y °C	[(9/5) y + 32] °C = x °F

QUICK INCH - CENTIMETER LENGTH CONVERSION

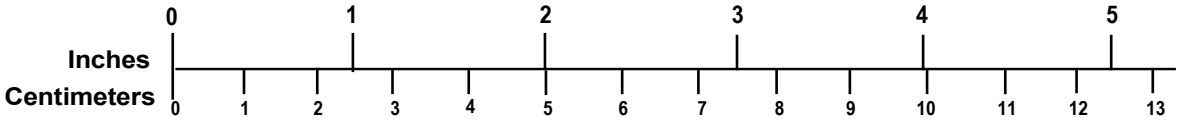

QUICK FAHRENHEIT - CELSIUS TEMPERATURE CONVERSIO

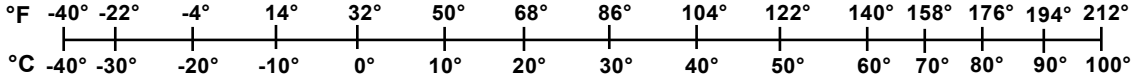

For more exact and or other conversion factors, see NIST Miscellaneous Publication 286, Units of Weights and Measures. Price $2.50 SD Catalog No. C13 10286

Updated 6/17/98

Acknowledgements

The authors appreciate the input from and discussions with the Federal Railroad Administration's Melissa Shurland and Jeffrey Gordon, the Volpe National Transportation Systems Center's Mark Gentile, Suzanne Horton and Bernard Kennedy IV, and industry representative Steve Roman from LTK Engineering.

Contents

Illustrations

Tables

Executive Summary

From September 19, 2018, to September 18, 2019, the Federal Railroad Administration (FRA) funded Jensen Hughes, Inc. to develop and evaluate methods to predict the heat release rate (HRR) history of rail car fires that includes all stages of the fire (i.e., growth, flashover, fully-developed and decay). The focus of this research initiative was to create fire modeling methods to predict the rail car HRR history and validate the models with experimental data.

Quantifying the HRR time history of a rail car fire is needed to design smoke control systems for tunnels and stations as well as assess the egress of passengers from the fire to a point of safety. The HRR is typically estimated using models that have limited validation for rail car applications. There is limited large-scale tests data existing in the public domain, and most tests do not include sufficient details for model validation. Smaller scale tests provide a means to cost-effectively quantify the geometric and design variations of the rail car on the HRR and provide validation data for models. However, the appropriate way to reduce the scale of the experiments so that the key physics are preserved has not been developed. In addition, the appropriate methods for modeling rail car fires has not been demonstrated.

Scaling laws, which are algebraic expressions that can be used to reduce the size of experiments while preserving the key physics of the problem, are developed in this research to allow for reducing the size of the rail car fire experiments. In addition, an initial assessment was performed to determine the appropriate method to provide detailed and simplified predictions of the HRR time history. It is recommended that a series of compartment fire experiments at different scales be conducted to generate data to validate the scaling laws and models formulated in this research.

A simplified model to predict the HRR time history was developed for use by designers and rail operators. This model uses empirical methods to predict the fire conditions based on the air flow into the rail car and interior surface area of the rail car. Material burning was predicted using a heat of gasification approach that allows for the burning rate to change based on the thermal exposure. This approach was found to account for the changes in air flow into the rail car, which other simplified methods do not capture. Additional comparisons need to be made with FDS simulation results and experimental data to further validate and refine the model.

1. Introduction

As the global population increases and the world moves increasingly toward energy-efficient methods of mass transit, including rail will need to continue to evolve to meet the increased transportation demand. To ensure the safety of passengers and crew in passenger rail cars in the United States, the Federal Railroad Administration (FRA) published Title 49 Code of Federal Regulations (CFR) Part 238 Section 103 [1] fire safety regulations in 1999 and 2002 that were intended to establish fundamental safety standards. Rail cars required to meet this standard included those ordered on or after September 8, 2000, or placed in service on or after September 9, 2002, as well as rail cars refurbished or overhauled after November 9, 1999, in which new materials were introduced in the rail car. Based on feedback from the industry through this rulemaking, FRA continues to invest in research to further improve passenger safety on rail cars and in railroad stations.

This research effort focused on developing methods to quantify the overall heat release rate (HRR) time history of passenger rail cars that includes all stages of the fire (i.e., growth, flashover, fully-developed and decay). Such HRR time history can be used to design smoke control systems for tunnels and stations. FRA funded Jensen Hughes, Inc. to conduct the research which occurred between September 19, 2018, and September 18, 2019. This report provides the results of the initial development of scaling laws for use in developing cost effective experimental measurements of rail car HRR measurements as well as modeling approaches for predicting rail car HRR.

1.1 Background

Research in the U.S. has primarily focused on reducing the flammability and smoke production of combustible materials used on rail cars to improve the fire safety of the rail car. These requirements are included to decrease the severity of the conditions that develop inside a rail car at the early stages of a fire and reduce the likelihood that an incipient fire will cause a rail car to reach flashover conditions. In addition to limiting flammability and smoke production to reduce the likelihood of a rail car reaching untenable conditions, rail systems that include underground stations and tunnels must also include smoke control systems that allow egress of passengers to a point of safety. Design of a smoke control system is typically based on the maximum HRR of a rail car fire, which is a fully-developed fire inside of a rail car. As a result, the rail car HRR time history is a critical consideration to ensure passengers are able to egress out of the rail car and reach a point of safety.

The U.S. conducted limited research on the contribution of materials to the overall HRR of a fully-developed rail car. In addition, standards include limited guidance for equipment owners and rail car manufacturers on considerations for predicting the HRR of fully-developed rail car fires to assist in making material selections. The use of the overall HRR of a rail car is not only used in design of smoke control systems for new stations and designs, it must also be considered for refurbished or replacement rail cars to ensure that the rail car HRR is within the design limits of the existing smoke control system. In previous design projects, it has been observed that including new materials on replacement rail cars can result in increasing the overall HRR of the rail car (despite meeting the flammability requirements) which can affect the performance of the existing smoke control system.

This report provides the initial research to validated models to support quantifying the HRR time history of a rail car fire. Scaling laws were successfully developed to predict the fire dynamics and material burning behavior in pre-flashover and fully-developed fires. Material burning was found to scale with heat release rate per unit area (HRRPUA), so dimensions should be scaled directly while thickness should remain constant to conserve energy. Froude modeling was found to be insufficient to scale fully-developed compartment fire dynamics due to it being developed to predict buoyancy driven flow behavior but not accounting for air flow effects on compartment fires. Instead, scaling laws conserving opening factor should be used to scale the ventilation opening (i.e., open window, open door) so that gas temperatures scale. The scaling laws were shown to be able to predict scaled compartment fire data from computer simulations using Fire Dynamics Simulator (FDS) within 10 percent. Additional comparisons with data are required to more completely demonstrate their use.

Failure of polycarbonate windows provides additional air for the fire which allows the fire HRR to increase significantly and provides additional smoke plumes. Both of these factors increase the amount of smoke produced by the rail car fire, increasing the ventilation requirements for the smoke control system. As a result, predicting this event is critical to provide accurate HRR time history and smoke control system design. A window failure model was developed using the finite element (FE) software Abaqus and successfully used to predict window failure in previous fire tests on polycarbonate windows. This model was used to explore scaling of windows, and it was shown that window thickness may need to be scaled based on the behavior of the full-scale window size. Due to the complexity of the scaling, algebraic scaling laws could not be developed. Instead, the Abaqus model was used to predict how windows would fail if the size was reduced.

Developing appropriate modeling methods to predict the HRR time history of a rail car fire is needed so that designers and operators can evaluate equipment and refine designs to improve safety. These models will be validated based on limited large-scale data as well as more extensive small-scale experimental data generated based on the scaling laws developed in this research. Methods for using the detailed computational model FDS were explored as well as a simplified fire dynamics model. The computational FDS was validated against fully-developed compartment fire data and then used to predict the HRR time history of a rail car fire. A detailed pyrolysis model that predicts solid material burning within FDS was found to be necessary to accurately account for the spatial variations and low oxygen concentration effects on the thermal exposure. Model trends are similar to those measured for similar rail cars in previous research; however, a full validation was not possible due to insufficient data on the interior finish materials. Additional validation of the model with experimental data is needed to further quantify the uncertainty of the model with actual fires.

1.2 Objectives

Quantifying the HRR time history of a rail car fire is a critical part of determining whether passengers can safely egress to a point of safety. This initial research effort focused on developing the analysis and modeling foundation to quantify the overall HRR time history of a rail car fire. Scaling laws, which are algebraic expressions that can be used to reduce the size of experiments while preserving the key physics of the problem, were developed to reduce the size of the rail car geometry that needs to be tested. Scaling of a rail car would be used to reduce the cost to conduct rail car experiments and allow for cost-effective experimental investigations to

understand the role of different parameters on the HRR. In addition, an evaluation took place of techniques for modeling the HRR time history of rail cars. An approach was developed for a detailed prediction of HRR using the computational fluid dynamics (CFD) model FDS. In addition, a simplified model was created to predict HRR that considers the effects of ventilation and rail car geometry on the fire dynamics. These models would be validated with the scaled rail car fire test data.

1.3 Overall Approach

The research was conducted in two parallel efforts. One effort was focused on developing the scaling laws for experiment design while the other effort was used to develop modeling techniques.

The approach for the scaling law effort was as follows:

- Literature review on material burning and window failure scaling
- Computer simulations to understand physics and support developing scaling laws
- Validation testing of scaling laws on burning materials and window failure
- Validation with computer simulations on all scaling laws

Developing methods for predicting the HRR history of rail cars using detailed and simple models was conducted using the following approach:

- Methods for determining material burning input data for FDS
- Validation of FDS fully-developed fire predictions with experimental data
- FDS simulations on full-scale using different modeling approaches
- Method for predicting material burning with simple model
- Development of simple model for fully-developed fire comparing with FDS simulations

1.4 Scope

This research is focused on developing and evaluating the scaling laws for reducing the size of experimental rail cars in testing and creating modeling methods to predict the HRR history of rail cars. Select scaling laws were validated with experimental results from this and other studies in the open scientific literature. In addition, the scaling laws were evaluated against FDS computer simulations to further demonstrate scaling law performance beyond the conditions of data in the literature. Modeling methods were evaluated for both detailed and simplified models. The detailed modeling used FDS and considered different types of material models to determine the most appropriate approach moving forward. In addition, a simplified model was developed that included basic fire dynamics and a simplified burning model. The model results were compared with computer simulations with FDS.

1.5 Organization of the Report

The report includes a series of five sections. Section 2 contains the research results on developing material burning and overall rail car fire dynamics scaling laws. In Section 3, the scaling laws for window failure due to fire exposure are presented and validated. The research

on detailed modeling of rail cars using FDS is provided in Section 4. Section 5 includes the research on a simplified modeling approach to predict the HRR history of a rail car. Section 6 contains the conclusions of the research as well as proposed future work.

2. Develop and Validate Fully-Developed Fire Scaling Laws

The following sections present the results of a systematic study to develop a scaling approach to predict fully-developed fire behavior in passenger rail car.

2.1 Background and Previous Work

Fire dynamics is a complex process involving fluid flow with chemical reactions, reaction of combustible materials, and multi-mode heat transfer. Complete scaling of these processes is not practical due to competing scaling requirements; however, it is often possible to gain insight and sufficient quantitative results using partial scaling [3]. The premise of partial scaling is to maintain similarity for key physics while relaxing similarity for less important aspects. Researchers have shown the behavior of a fully-developed fire is controlled by fuel burning rate, the availability of oxygen/ventilation, and thermal losses [4]. Partial scaling intended to predict the HRR of fully-developed fires should maintain similarity of these parameters.

Froude modeling-based scaling has traditionally been used in fire applications [3]. Froude modeling focuses on scaling the dynamics of the fire plume (matching the gas temperature and velocity of the buoyant plume), but relaxes the similarity of the solid boundary [3]. Researchers have presented an extensive overview of Froude scaling for tunnel and rail car applications [5]. Figure 2-1 shows the list of scaling correlations developed for the model tunnel using Froude scaling. This approach is designed to predict the growth of the initial fire; however, it is difficult to maintain the fuel burning rate and thermal losses necessary to model a fully-developed fire since the similarity of the solid boundary is relaxed. The authors in [5] used different materials (type and thickness) between the model scale and full scale to compensate for this limitation; however, the competing material properties make it difficult to apply this method.

Surface energy-based approaches scale the burning behavior of materials by maintaining the HRRPUA of the fuel, but relaxes the similarity of the fire plume [6]. This scaling approach has been used to predict the pre-flashover conditions in a National Fire Protection Association (NFPA) 286 room [7]–[9]. A key advantage of this approach in predicting fully-developed fire conditions is the fuel burning rate and thermal losses are maintained between the model scale and full scale by using the same materials. However, the availability of oxygen does not directly scale in this approach. Researchers have presented a relaxed geometric scaling on the door to maintain the availability of oxygen based on flow work through the door [7]–[9]. Bullen et al. (1976) showed this scaling approach can predict gas temperatures and species concentrations from a single gas burner. Lee (1985) and Dingyi (1987) showed this scaling approach can predict the onset of flashover with combustible lining materials.

These studies have not examined the capability of these scaling approaches to predict the conditions of a post-flashover, fully-developed fire. In addition, the models examined in the literature survey have been limited to a single ventilation source. The objective of this study was to develop a scaling methodology to predict the conditions in a fully-developed fire under complex ventilation conditions.

Type of unit	Scaling
Heat Release Rate (HRR) (kW)	$\dot{Q}_M / \dot{Q}_F = (l_M / l_F)^{5/2}$
Velocity (m/s)	$V_M / V_F = (l_M / l_F)^{1/2}$
Time (s)	$t_M / t_F = (l_M / l_F)^{1/2}$
Energy (kJ)	$E_M / E_F = (l_M / l_F)^3$
Mass (kg)*	$m_M / m_F = (l_M / l_F)^3$
Temperature (K)	$T_M / T_F = 1$
Gas concentration*	$Y_M / Y_F = 1$
Pressure (Pa)	$P_M / P_F = l_M / l_F$
Fuel mass burning rate (kg/m^{2}s)	$(\dot{m}''_f \Delta H_c)_M / (\dot{m}''_f \Delta H_c)_F = (l_M / l_F)^{1/2}$
Fuel density (kg/m^3)	$(\rho \Delta H_c)_M / (\rho \Delta H_c)_F = 1$
Fuel heat of pyrolysis	$(\Delta H_c / L_p)_M / (\Delta H_c / L_p)_F = 1$
Thermal inertia (kW^2·s·m^{-4}·K^{-2}))	$(k \rho c)_{s,M} / (k \rho c)_{s,F} \propto (l_M / l_F)^{3/2}$
Thickness (m)	$(k / \delta)_{s,M} / (k / \delta)_{s,F} \propto (l_M / l_F)^{1/2}$
Conduction heat flux (kW/m^2)	$\dot{q}''_{k,M} / \dot{q}''_{k,F} = (l_M / l_F)^a (0 \le a < 1/2)$
Radiation heat flux (kW/m^2)	$\dot{q}''_{r,M} / \dot{q}''_{r,F} = (l_M / l_F)^a (0 \le a < 1/2)$
Convection heat flux (kW/m^2)	$\dot{q}''_{c,M} / \dot{q}''_{c,F} = (l_M / l_F)^a (-1/4 \le a < 1/5)$

*assuming $\Delta H_{c,F} = \Delta H_{c,M}$.

Figure 2-1. Scaling correlations for a model tunnel based on Froude modeling [1]

2.2 Burning Scaling Law

Computer simulations using FDS version 6 of materials in a cone calorimeter were used to examine the impact of material thickness and exposed surface area on material burning rate for use in assessing the appropriate scaling laws. The model simulated cone calorimeter testing of polymethylmethacrylate (PMMA) exposed to a heat flux of 50 kW/m^2 (4.4 Btu/s-ft^2). The full-scale sample size was 0.101 m x 0.101 m (4.0 in. x 4.0 in.) with a thickness of 6.35 mm (0.25 in.). The area and thickness were geometrically scaled by one-half and one-quarter length scale. For a given exposure level, the HRR was found to scale by

$$\frac{\dot{Q}_M}{\dot{Q}_F} = \left(\frac{l_M}{l_F}\right)^2 \qquad (2\text{-}1)$$

where $\dot{Q}$ is the HRR (subscripts M and F correspond to the model scale and full-scale), l_M is the model length scale, and l_F is the full-scale length scale. This also indicates that the HRRPUA of the material is preserved regardless of scale for a given exposure level. In order to preserve the total energy, time was scaled based on the material thickness

$$\frac{t_M}{t_F} = \left(\frac{\delta_M}{\delta_F}\right) \qquad (2\text{-}2)$$

where t is time and δ is the material thickness. Figure 2-2a shows the FDS simulation. The HRR for the full thickness as well as model scaled thicknesses of one-half and one-quarter are compared in Figure 2-2b. Overall the time-resolved HRR profile at each scale agrees well. This shows the following:

- The HRRPUA is independent of scale (since the HRR is scaled with area according to Equation 2-1).
- The primary impact of material thickness on the HRR curve is the burning duration.
- The same materials can be used in the full-scale and model-scale if the surface area is scaled geometrically, the same material thickness is used at each scale, and the thermal exposure is the same.

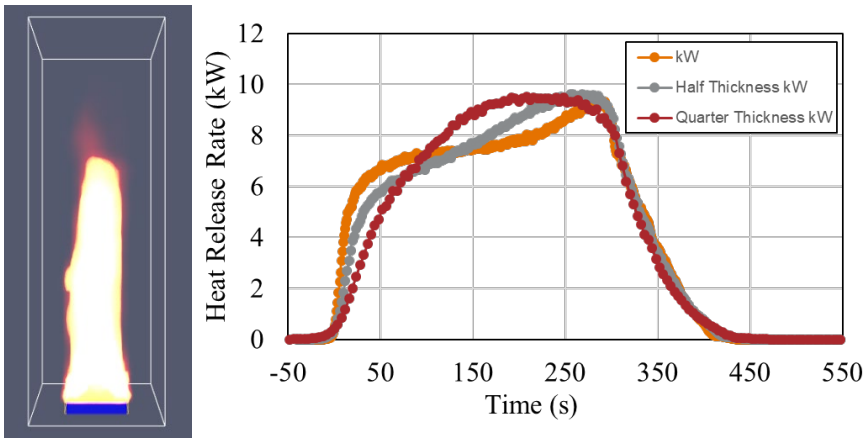

(a) **(b)**

Figure 2-2. Cone calorimeter material burning scaling; (a) FDS model, (b) heat release rate

2.3 Fully-Developed Fire Scaling Law Comparison

2.3.1 Fully-Developed Fire Scaling Laws

The fundamental basis of the burning scaling presented in Section 2.2 is that the thermal exposure to the materials must be the same in the reduced scale as in the full-scale. A set of scaling laws to maintain the thermal exposure of a fully-developed compartment fire based on surface energy, oxygen availability, and burning duration was developed in this work. The overall compartment geometry is scaled by the desired length scale

$$s = \left(\frac{l_M}{l_F}\right) \tag{2-3}$$

where s is the desired reduced scale, l_M is the model length scale, and l_F is the full-scale length scale. The initiating fire geometry is scaled geometrically such that the HRRPUA is equal between the full-scale and reduced scale and the HRR is scaled according to Equation 2-1. The oxygen availability needs to be scaled to describe the behavior of fully developed fires. The availability of oxygen can be related to the HRR as

$$\dot{Q} = \dot{m}_{air}\Delta H_{c,O_2} \tag{2-4}$$

where $\dot{m}_{air}$ is the mass flow rate of air into the compartment and $\Delta H_{c,O_2}$ is the fuel heat of combustion per unit mass of oxygen. Bullen showed the maximum $\dot{m}_{air}$ in a compartment fire is related to the size of the ventilation by the Equation 2-5

$$\dot{m}_{air} = 0.5(WH)H^{1/2} \quad (2\text{-}5)$$

Where W is the width of the ventilation and H is the height of the ventilation [6]. Since the same fuel materials are used in the full-scale and model scale, equations 2-1 through, 2-4, and 2-5 can be re-arranged to provide the expression below relating the length scales to the door geometry

$$\frac{l_M^2}{(W_M H_M^{3/2})} = \frac{l_F^2}{(W_F H_F^{3/2})} \quad (2\text{-}6)$$

Unfortunately, Equation 2-6 is not satisfied in direct geometric scaling. Thus, the size of the ventilation must be scaled differently between the full-scale and reduced scale to scale the oxygen available for combustion in the compartment. A scaling law for the ventilation height can be defined as

$$\frac{H_M}{H_F} = \left(\frac{l_M}{l_F}\right)^a \quad (2\text{-}7)$$

and for the ventilation width as

$$\frac{W_M}{W_F} = \left(\frac{l_M}{l_F}\right)^b \quad (2\text{-}8)$$

where the coefficients a and b can be related through Equation 2-6 as

$$b = 2 - \frac{3}{2}a \quad (2\text{-}9)$$

The results of this study showed it was preferable to increase the height of the ventilation and maintain the width. However, for large aspect ratio openings (such as doors) it is often not possible to scale the height enough to maintain the oxygen availability without also scaling the width due to the height of the ceiling. The maximum a for Equation 2-7 can be calculated using the equation

$$a_{max} = 1 - \frac{\ln(H_F/H_{F,max})}{\ln(l_M/l_F)} \quad (2\text{-}10)$$

Where $H_{F,max}$ is the ceiling height inside the compartment adjacent to the opening. Thus, the following procedure is used to scale each ventilation path:

- Determine a' with an assumed $b = 1$ in Equation 2-9
- Determine a_{max} based on Equation 2-10 based on the specific geometry and desired scaling ratio
- Calculate b using Equation 2-9 with a=max(a', a_{max})
- Calculate opening height and width using equations 2-7 and 2-8

2.3.2 Verification of Computer Simulations

Computer simulations in FDS, version 6 were used to examine different scaling methodologies. The simulations were conducted with a grid size calculated based on the non-dimensional fire

size, as recommended in the FDS user guide. The grid resolution was calculated using the equation

$$\frac{D^*}{dx} = 10 \tag{2-11}$$

where *dx* is the grid size and *D** is the non-dimensional fire size, calculated using the equation

$$D^* = \left(\frac{\dot{Q}}{\rho_\infty c_p T_\infty \sqrt{g}}\right)^{\frac{2}{5}} \tag{2-12}$$

where ρ_∞ is the ambient air density, C_p is the ambient air specific heat capacity, T_∞ is the ambient air temperature, and *g* is the acceleration due to gravity. The numeric value of 10 in Equation 2-11 corresponds to a moderate mesh resolution, which adequately resolves the gas temperatures. In addition, grid cells were added outside of the compartment to ensure appropriate flow field development. The computational domain was extended 4 grid cells beyond walls with no ventilation, 20 grid cells beyond walls with ventilation, and 20 grid cells above the compartment.

The accuracy of the computer simulations at full scale and reduced scale was assessed by reproducing experiments performed by the National Institute of Standards and Technology (NIST) at two different scales. The full-scale experiment used an NFPA 286 room with a gas burner in the center of the room with a HRR of 2,700 kW (2,559 Btu/s). Gas temperatures were measured 10 cm below the ceiling in the front-right corner (50 cm (2.0 in.) from the front and side wall) and the back-right corner (50 cm (2.0 in.) from the back and side wall). The FDS model of the full-scale experiment is shown in Figure 2-3a. Gas temperatures from the experiment and computer simulation are compared in Figure 2-3b. The FDS predictions of gas temperature for the full-scale were within 10 percent of experimental measurements, which is acceptable deviation based on other FDS validation.

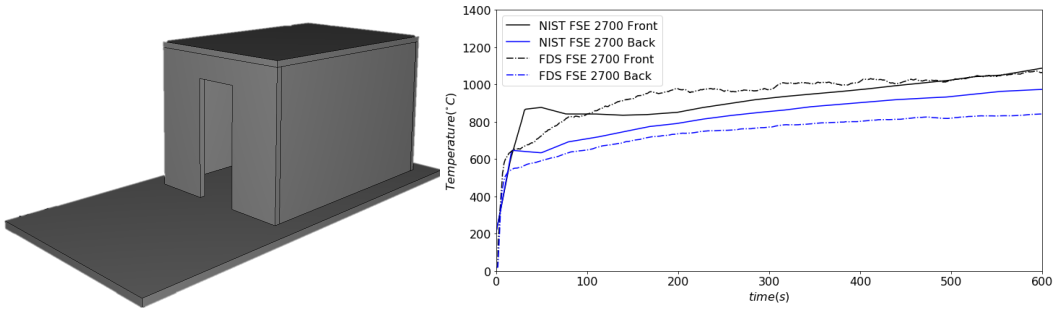

(a) **(b)**

Figure 2-3. (a) FDS model of NIST full-scale compartment experiment: (b) gas temperatures from the FDS model and experiment

The small-scale experiment used a 40 percent scaled NFPA 286 room with a larger door, 0.48 m x 0.81 m (1.57 ft x 2.66 ft). The gas burner was in the center of the room with a HRR of 432 kW (409 Btu/s). Gas temperatures were measured 4 cm (1.6 in.) below the ceiling in the front-right corner (20 cm (7.9 in.) from the front and side wall) and the back-right corner (20 cm (7.9 in.) from the back and side wall). Figure 2-4a shows the FDS model of the small-scale experiment.

Figure 2-4b compares gas temperatures from the experiment and computer simulation. The FDS predictions of gas temperature for both the full-scale and small-scale were within 15 percent of experimental measurements, which is acceptable based on other FDS validation.

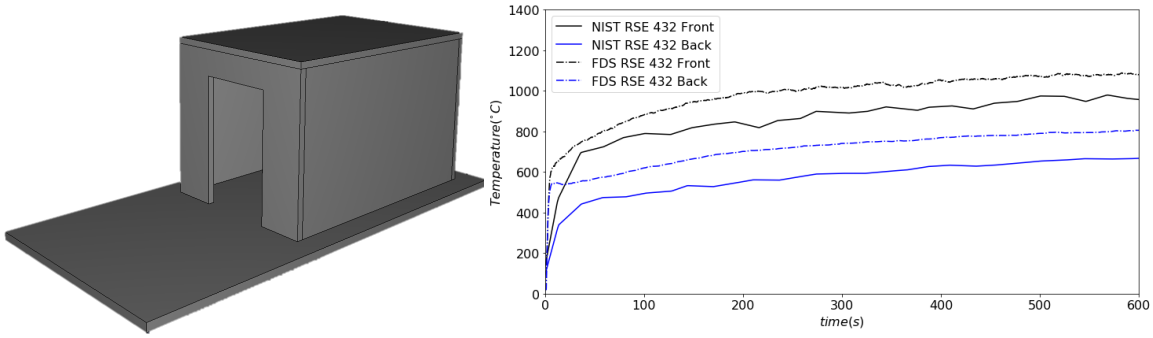

(a) **(b)**

Figure 2-4. FDS model of NIST small-scale compartment experiment: (a) geometry and (b) compartment temperatures

2.3.3 Fully-Developed Scaling Law Comparison

Predictions of gas temperature using the previously presented scaling laws were compared with gas temperature predictions using Froude scaling. All temperatures were predicted using FDS with different geometric detail based on the type of scaling method used. The full-scale computer simulation considered a 5 m x 5 m x 5 m (16.4 ft x 16.4 ft x 16.4 ft) with a 1.25 m x 2.50 m (4.1 ft x 8.2 ft) door with a gas burner in the center of the room with a fixed HRR. The HRR was set at 1,350 kW (1,280 Btu/s) to examine the scaling for pre-flashover fire and set at 2,700 kW (2,559 Btu/s) to examine the scaling during a post-flashover fire. In each scaling approach, the compartment geometry was scaled 1:5. The FDS model for the full-scale compartment and reduced-scale compartment is shown in Figures 2-5.

Gas temperatures in the back-right corner of the compartment are compared between the full-scale and each reduced scale approach in Figure 2-6. The black line is the gas temperature from the full-scale computer simulation. The blue dash-dot line is the gas temperature of the reduced scale model using Froude scaling. The red dashed line is the gas temperature using the scaling approach discussed in Section 2.3.1. Table 2-1 summarizes the median percent difference between the gas temperatures in the full-scale and each reduced scale. The percent difference in upper layer and mid-height temperature from the proposed scaling approach is between 5–10 percent; whereas the percent difference using the Froude scaling approach is between 15–20 percent. The gas temperatures in the lower layer from the proposed scaling approach were between 25–40 percent different; whereas the percent difference using the Froude scaling approach was between 5–15 percent. Since the upper layer temperature is more critical in quantifying the behavior of fully-developed fires, these results indicate the proposed scaling approach will be more representative of full-scale behavior than the Froude scaling approach.

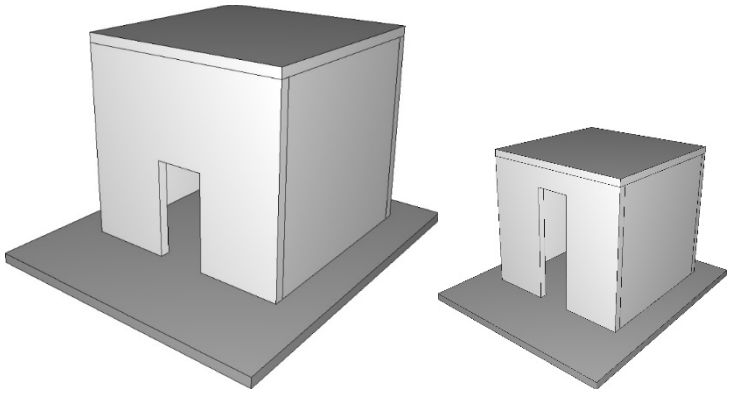

(a) **(b)**

Figure 2-5. FDS models from fully-developed scaling law development computer simulations for a) full-scale compartment and b) 1:5 scale compartment

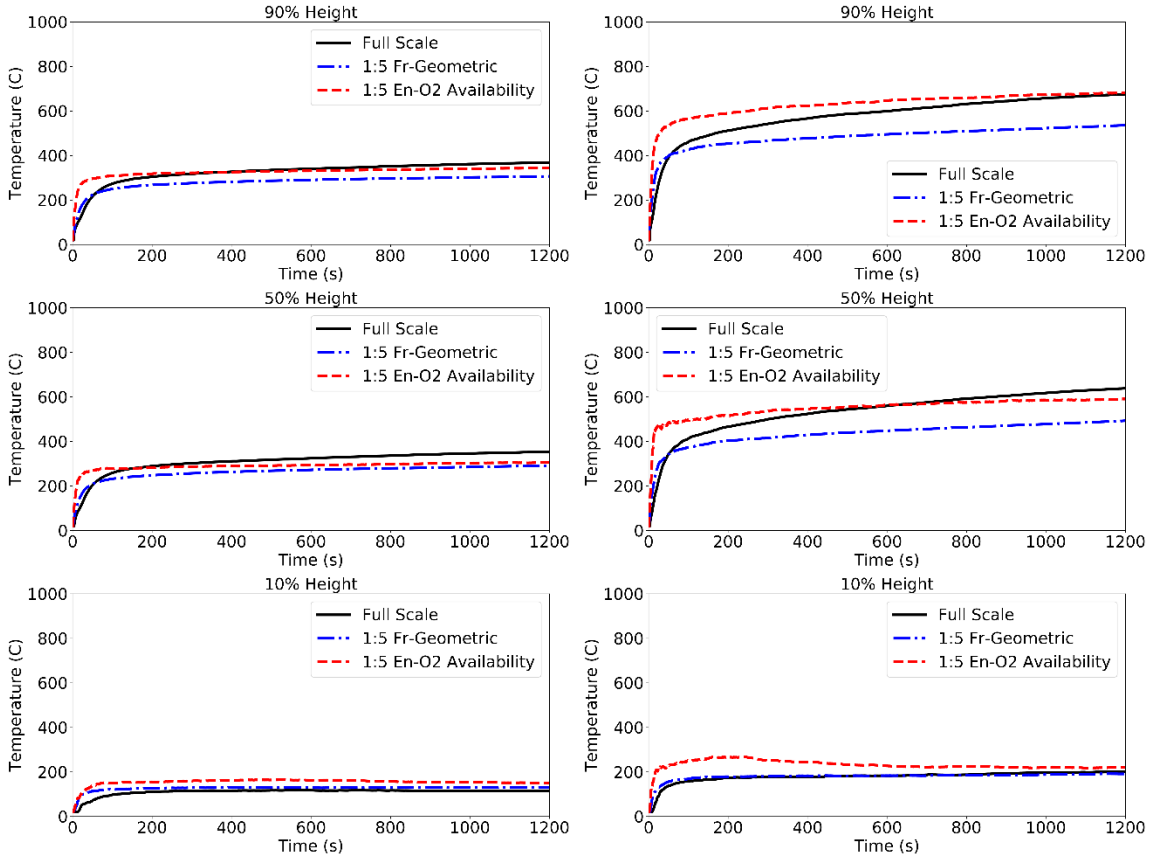

(a) **(b)**

Figure 2-6. Comparison of gas temperature predictions at different elevations for different scaling approaches a) with a pre-flashover fire and b) with a post-flashover fire

Table 2-1. Percent difference in gas temperature from full-scale using different scaling approaches

	Froude Scaling		Surface Energy Scaling	
Height Percent	1,350 kW	2,700 kW	1,350 kW	2,700 kW
90 percent (Upper layer)	14.7 percent	17.7 percent	4.3 percent	7.7 percent
50 percent (Middle)	16.2 percent	20.3 percent	10.4 percent	4.9 percent
10 percent (Lower layer)	12.9 percent	2.9 percent	38.7 percent	24.4 percent

2.4 Using Scaling Laws for Fully-Developed Fire Applications

Generally, scaling studies of compartment fires have limited the analysis to rooms with single ventilation paths. However, fully-developed fires in passenger rail cars often have multiple openings available for the transport of air and smoke (such as doors and windows). The scaling laws presented in Section 2.3 were applied to predict gas temperatures in a fully-developed fire in a baseline NFPA 286 room and a modified NFPA 286 room with an additional window on each side wall to investigate the impact of multiple ventilation paths on the scaling analysis.

The full-scale model dimensions were 3.66 m x 2.44 m x 2.44 m (12 ft. x 8 ft. x 8 ft.) with a door size of 0.76 m x 2.03 m (2.49 ft. x 6.65 ft.). The initiating fire was a gas burner with a fixed HRR placed in the center of the room. HRRs were chosen to produce pre-flashover, 300 kW (284 Btu/s), and post-flashover, 3,000 kW (2,840 Btu/s), fire conditions. Model scales at 1:2 (one-half) and 1:5 (one-fifth) were considered for each NFPA 286 room. Figure 2-7 shows the full-scale and 1:5 scale baseline NFPA 286 room models. Figure 2-8 shows gas temperatures in the back-left corner for the baseline NFPA 286 room model at full scale, 1:2 scale, and 1:5 scale. Table 2-2 summarizes the median percent difference in gas temperature of each reduced scale from the full-scale gas temperatures. The full-scale and 1:5 scale modified NFPA 286 room models with two side windows (0.6 m x 0.6 m (2 ft. x 2 ft.) each) are shown in Figure 2-9, the gas temperatures in the back-left corner are shown in Figure 2-10, and the median percent difference in gas temperature is summarized in Table 2-3.

Overall, the upper-layer gas temperature predictions from the surface energy-based scaling were within 10 percent for the fully-developed fires with both the baseline and the modified NFPA 286 geometry. These results show that the scaling approach presented in Section 2.3 could predict the full-scale gas temperatures with multiple ventilation paths.

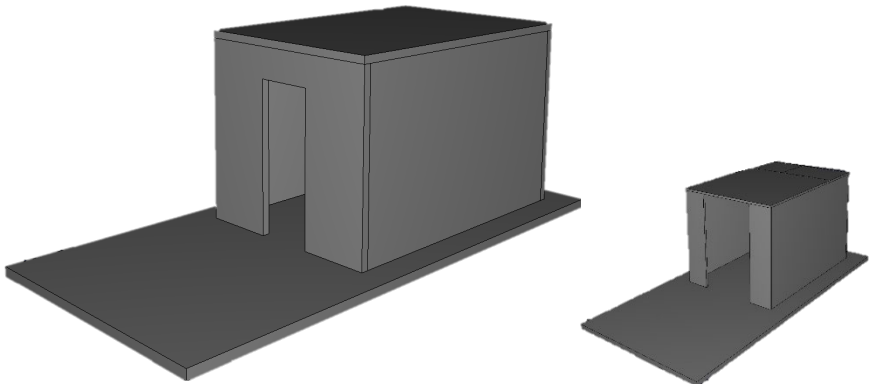

(a) **(b)**

Figure 2-7. FDS models from NFPA 286 baseline single door compartment scaling law computer simulations for a a) full-scale compartment and b) 1:5 scale compartment

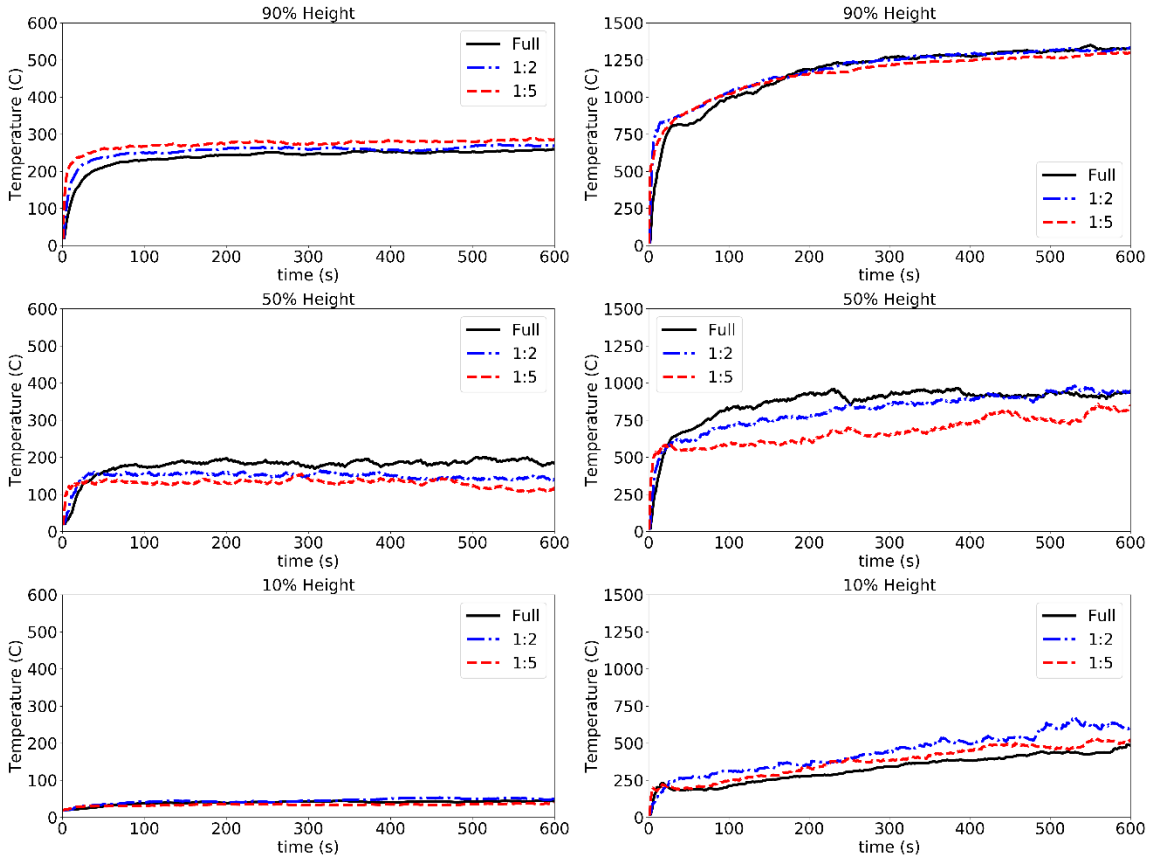

(a) **(b)**

Figure 2-8. Comparison of gas temperature predictions at different elevations for NFPA 286 baseline compartment with a single door at different scales a) with a pre-flashover fire and b) with a post-flashover fire

Table 2-2. NFPA 286 baseline model percent difference in gas temperature at different scales

	1:2 Scale		1:5 Scale	
Height Percent	300 kW	3,000 kW	300 kW	3,000 kW
90 percent (Upper layer)	5.7 percent	1.1 percent	11.4 percent	3.2 percent
50 percent (Middle)	21.6 percent	7.2 percent	29.7 percent	25.3 percent
10 percent (Lower layer)	11.1 percent	33.1 percent	22.1 percent	13.7 percent

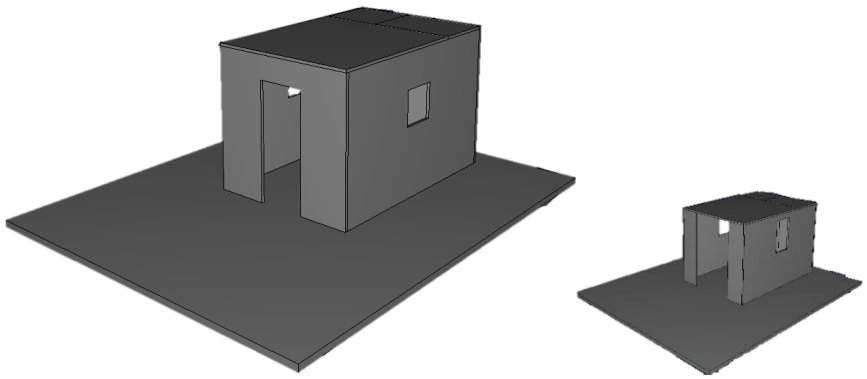

(a) **(b)**

Figure 2-9. FDS computer simulation models from modified NFPA 286 compartment with a door and windows at a) full-scale and b) 1:5 scale

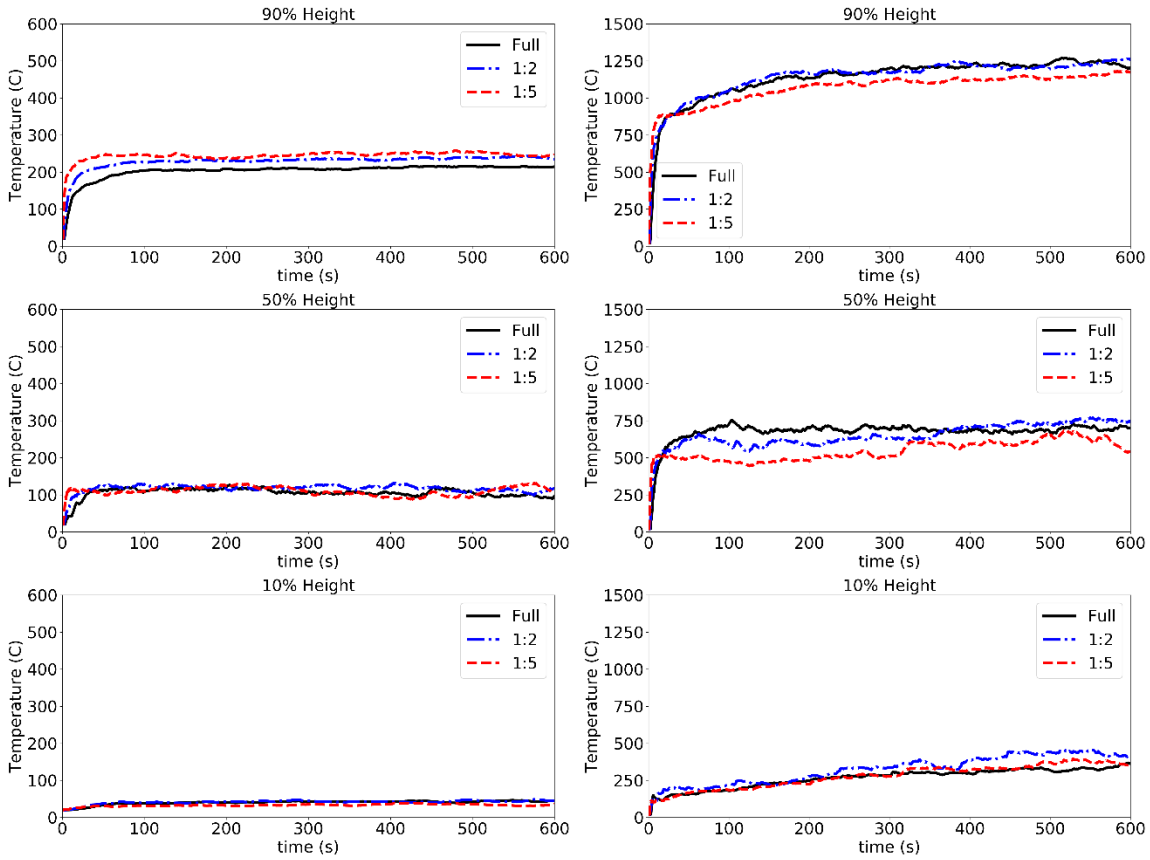

Figure 2-10. Comparison of gas temperature predictions for the modified NFPA 286 with a door and windows at different scales a) with a pre-flashover fire and b) with a post-flashover fire

Table 2-3. NFPA 286 modified model percent difference in gas temperature at different scales

	1:2 Scale		1:5 Scale	
Height Percent	300 kW	3,000 kW	300 kW	3,000 kW
90 percent (Upper layer)	11.5 percent	1.8 percent	16.1percent	6.9 percent
50 percent (Middle)	7.7 percent	8.2 percent	6.4 percent	21.5 percent
10 percent (Lower layer)	5.9 percent	21.6 percent	20.4 percent	5.9 percent

2.5 Section Summary

This study focused on developing scaling laws to predict full-scale fire behavior in pre-flashover and fully-developed fires from a reduced scale model. Computer simulations in FDS were used to generate full-scale and reduced-scale data to develop and validate the approach. The developed scaling approach was able to predict upper gas layer temperatures in the full-scale

model within 10 percent for complex ventilation conditions. The following are the conclusions from the results:

- The same materials can be used in the full-scale and reduced-scale as long as the surface area is scaled geometrically, the same material thickness is used at each scale, and the thermal exposure is the same.

- Similar thermal exposure (gas temperatures) can be achieved by using the scaling laws developed in this work where the initiating fire is scaled by Equation 2-1 and the availability of oxygen is scaled by adjusting the height and widths of openings using equations 2-7 to 2-10.

The next steps in developing this methodology include the following:

- Conduct fire experiments to demonstrate the scaling laws in scaled rooms without combustible boundaries considering both a single ventilation path (one door) as well as a multiple ventilation paths (door and windows)
- Conduct fire experiments to demonstrate the scaling laws in scaled rooms with combustible boundaries considering both single and multiple ventilation paths

3. Develop and Validate Window Burn Through Scaling Laws

Fire-induced window failure, or breach, has a significant effect on the HRR of an interior rail car fire as it creates pathways for oxygen to enter the rail car and combustion gases to leave. This is especially true in ventilation limited fires. Thus, obtaining accurate window failure times in simulations and reduced-scale experiments is important in accurately predicting the HRR of an actual fire.

3.1 Background and Previous Work

Previous testing of rail car windows under fire exposure has shown failure of the window glazing (e.g., polycarbonate) can occur at heat fluxes as low as 25 kW/m^2 (2.2 Btu/s-ft^2) [10]. The failure was observed as a hole forming in the near the center of the polycarbonate window glazing and not at the edges where the gaskets and frame were located. This testing has also shown how the in-plane geometry of the window impacts the failure conditions. The temperature responses shown in Figure 3-1 highlight the geometric effects. In this figure, Type A windows were 0.5 m (1.52 ft.) tall and 0.56 m (1.84 ft.) wide while Type B windows were 0.6 m (1.97 ft.) tall and 1.42 m (4.66 ft.) wide. Both polycarbonate windows were 12.7 mm (0.5 in) thick. Failure times and backside temperatures were reduced for the larger window.

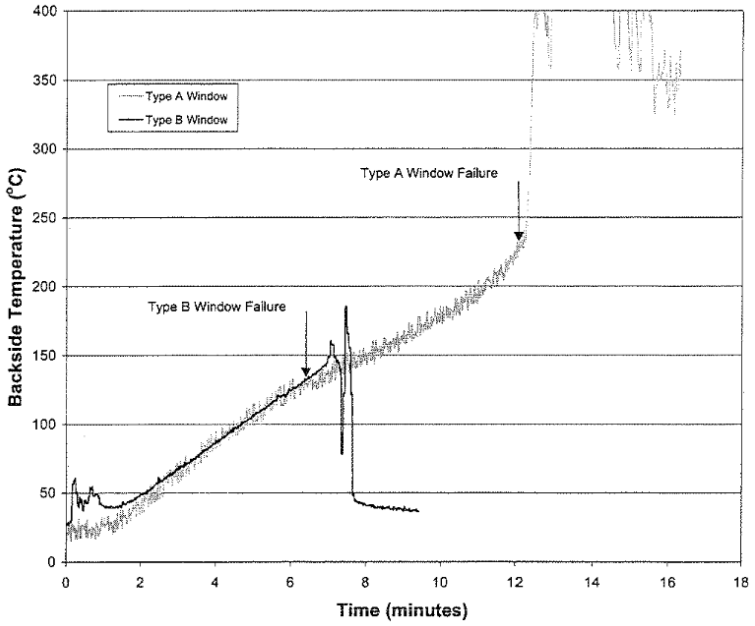

Figure 3-1. Backside temperature response of two different window sizes exposed to 30–40 kW/m^2 by Strege et al. [10]

This geometry dependency points to a thermo-mechanical rupture failure mechanism rather than a purely thermal event such as melting. This fire-induced thermo-mechanical rupture behavior has been previously observed in aluminum alloy panels [11] where rupture of the panels occurs at temperature below the material melting temperature. While this thermo-mechanical rupture mechanism causes failure for larger panels or exposures, smaller exposures cause rupture via melting because stresses at the failure location are lower for smaller exposures [12]. This

necessitates the need to consider both failure mechanisms when predicting the fire-induced rupture of window panels at full and reduced scale.

3.2 Multi-Mechanism Window Failure Model

The implemented failure model considered the melting and rupture of the window as two independent mechanisms and failure of the window is considered to have occurred when either mechanism occurs. The simpler of the two mechanisms is melting, as this is a strictly thermally based mechanism. While the behavior of polycarbonate is rather complex above the glass transition temperature of 145 °C (293 °F), the melting temperature of typical polycarbonate products is listed as 225 °C (437 °F). Thus, if the entire thickness at any location on the window exceeds this temperature, the window is considered failed via melting. Additionally, if any location within the thickness exceeds this temperature, it is modeled as melted material that does not contribute to stiffness of the model. The effective weight of this material, however, cannot be removed given the current model capabilities.

The more difficult failure mechanism to model is the creep-based rupture mechanism, which is failure that occurs when there is elevated temperature and low load such as self-weight. Several numerical models have been introduced in the engineering literature to predict creep rupture. The Larson-Miller Parameter (LMP) method was selected in this work [13]. The LMP is a temperature-independent predictor of creep rupture time that is only a function of the applied stress. LMP and rupture time are related by

$$t_r = 10^{\frac{P_{LM}}{T} - C} \tag{3-1}$$

Where t_r is the rupture time in seconds, P_{LM} is the LMP, T is the temperature in Kelvin, and C is a material constant. The form of the LMP as a function of stress is determined through a series of standard uniaxial tensile creep tests as discussed in the following section.

The LMP is designed to predict creep rupture under constant stress and temperature conditions. Because a window exposed to fire undergoes temperature and stress changes as function of time, a Palmgren-Miner rule was used predict failure under the variable conditions. This implementation in a time-discretized FE analysis is

$$f_i = f_{i-1} + \frac{\Delta t}{t_r} \tag{3-2}$$

where f_i is the life fraction at the end of the current step, f_{i-1} is the life fraction at the beginning of the current step, Δt is the analysis timestep, and t_r is the rupture time predicted using the current temperature and stress. The life fraction at the start of the analysis is zero (0) and failure is considered to occur when the life fraction reaches a value of one (1).

3.3 Material Properties and Characterization

Several material dependent parameters are needed to accurately implement the creep rupture model. These parameters were determined using a series of uniaxial tension creep tests of polycarbonate. Test temperatures were conducted at temperatures as low as 160 °C (320 °F) because this is the lowest temperature in which failure was experimentally observed by Strege et al. [10]. Test temperature were as high as 180 °C (356 °F). While failure was experimentally observed above this temperature, decomposition of the material began to occur above this

temperature so material testing could not be performed. Instead, a temperature dependent model was used with results extrapolated up to the melting temperature of 225 °C (437 °F).

Creep test samples consisted of 12.7 mm (0.5 in.) diameter, 0.3 m (1.0 ft.) long round specimens heated in a vertically oriented tube furnace. The samples were hung from above using press fittings outside of the heated zone. A static load was applied at the bottom of the sample just below the heated zone by hanging weights. A series of marks along the side of each sample at 12.7 mm (0.5 in.) intervals allowed for sample elongation to be measured via video extensometer through a small slit in the side of the furnace. Figure 3-2 shows the experimental setup.

The temperature of the polycarbonate could not be accurately measured during each test because mounting a thermocouple would affect the creep response and the transparent nature of the material prohibits accurate infrared (IR) measurement. Instead, a series of thermal calibration tests were run before the experiments in which an unloaded sample was heated within the furnace. The sample temperature was measured with a mounted thermocouple and the IR emission was measured with an IR camera to correlate the two measurements. IR measurements taken during each experiment and this correlation were then used to determine sample temperature for each creep test.

Figure 3-2. Experimental setup for uniaxial tensile creep tests of polycarbonate at elevated temperatures

The typical tensile creep response of the polycarbonate provided in Figure 3-3 shows the material undergoing minimal primary creep with significant secondary and tertiary creep regimes. To model this response, a modified Kachonov-Robatnov creep model was used [14] [15]. The use of the Kachanov-type creep model works well for materials that exhibit large secondary and tertiary creep regimes and fits well with the life fraction approach used to characterize failure. Creep strain increments are calculated within the FE model as

$$\Delta\varepsilon = \dot{\varepsilon}_{II}\Delta t(1-f)^{1/\lambda-1} \tag{3-3}$$

where

$$\dot{\varepsilon}_{II} = A \sinh (B\sigma)^n e^{-Q/RT} \tag{3-4}$$

where f is the current life-fraction value, σ is the deviatoric portion of the stress tensor, R is the universal gas constant, T is the temperature in Kelvin, and λ, A, B, n, Q are material constants.

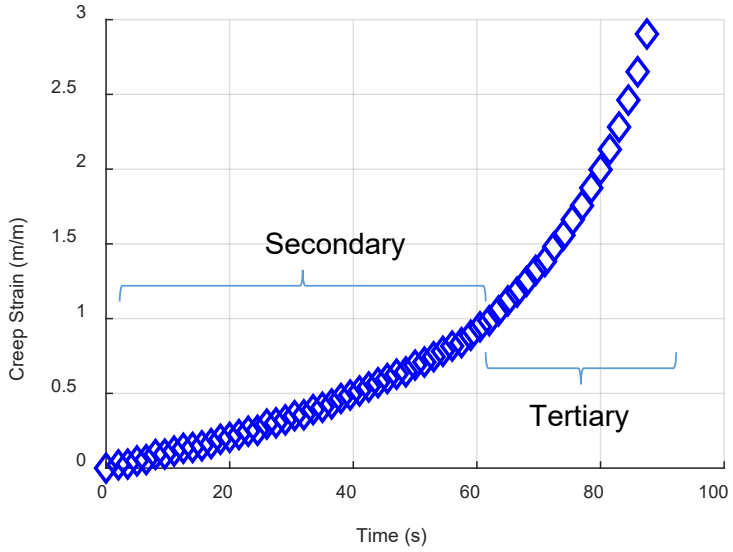

Figure 3-3. Typical experimental tensile creep curve for polycarbonate above the glass transition temperature showing the location of the secondary and tertiary creep regimes

Multi-variable non-linear regression of the creep curves was used to the value of each of the material constants. Additionally, a linear relationship between LMP and deviatoric stress was assumed. Using this model, the LMP was calculated as

$$P_{LM} = -0.0019\sigma + 5670 \tag{3-5}$$

for stresses up to 200 kPa (29.0 psi). This low limit is because when a window is locally heated, stresses in the window at the failure point are relaxed away due to plasticity and creep resulting in low stresses at the failure location. The values of the remaining material constants are provided in Table 3-1. Using this complete creep model, the prediction of the creep tests was conducted. Figure 3-4 shows typical experimental and modeled curves for select temperature and stress combinations. Some experimental curves are not well predicted by the creep model due primarily to error in the rupture time prediction. This error stems from the high degree of variability in experimentally observed rupture time.

Table 3-1. Material constants for elevated temperature creep model of polycarbonate for the creep model in equations 3-3 and 3-4

Parameter	Value
λ	1.9323
A	$2\ x\ 10^{14}$
B	$7.37\ x\ 10^{-6}$
n	0.892
Q	138000

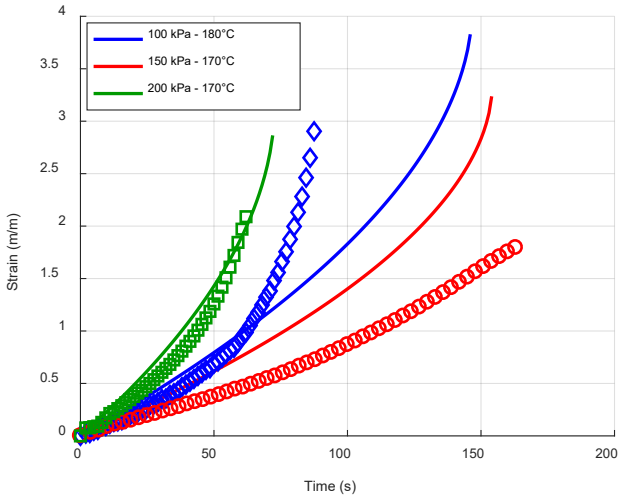

Figure 3-4. Comparison of experimentally observed (symbols) and model (lines) predicted creep behavior of polycarbonate at select temperatures and stresses

3.4 Burn Through Model Validation

The rupture model was validated against the experimental data previously published by Strege et al. [10]. These experiments consisted of a 12.7 mm (0.5 in) thick polycarbonate window exposed to radiant heat flux from a propane line burner. Figure 3-5 provides the previously published experimental setup. Two window sizes were used in these tests: a 0.56 m (22 in) wide by 0.5 m (19.7 in) high window and a 1.42 m (55.9 in) wide by 0.6 m (23.6 in) wide window. Models of each of the line burner experiments were developed and compared to experimental results to validate the model. Sequentially coupled thermal and mechanical models were generated and run using the commercially available FE software package Abaqus. Abaqus is a well-established FE analysis package capable of conducting geometrically and materially non-linear thermal and mechanical FE analyses. Abaqus also has an available library of user subroutines that can be used to customize the model response. These routines were used to implement the polycarbonate creep and failure models into the analyses.

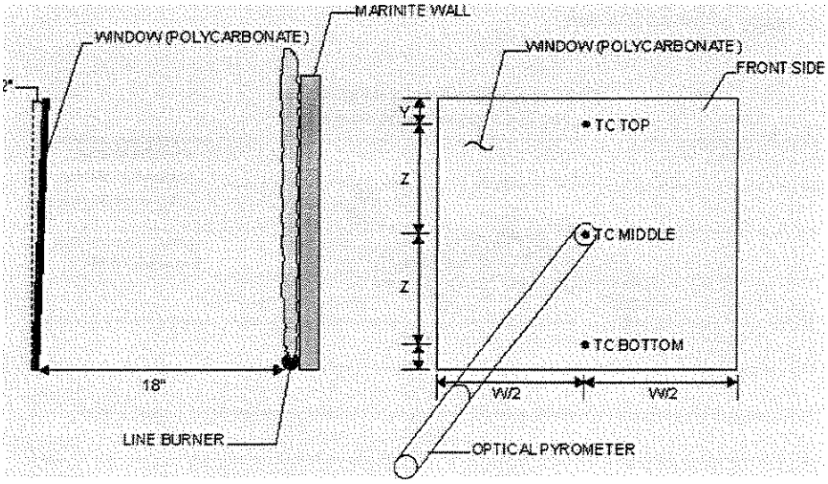

Figure 3-5. Schematic of line burner test setup for polycarbonate window failure by Strege et al. [10]

Heat flux into the polycarbonate window was experimentally measured at three elevations. This vertically varying heat flux profile was used in the thermal models of the windows while no horizontal heat flux distribution was considered. The thermal models consisted of the polycarbonate window and the steel mounting frame on the exposed side of the window. This allowed for heat to flow between the frame and window and blocked the perimeter of the window that is under the frame from the applied heat flux causing cooler edges on the window. Gaskets were not included in the experimental setup and therefore not included in the simulations. The window and frame were modeled with two-dimensional shell elements due to the thin nature of the elements. Each surface had nine section points through the thickness and an in-plane mesh seed of 12.7 mm (0.5 in). Temperature dependent thermal properties of the polycarbonate and steel frame were used in the analysis. Figure 3-6 shows the geometry and mesh used for the analysis of the 0.56 m (22 in) wide by 0.5 m (19.7 in) high window.

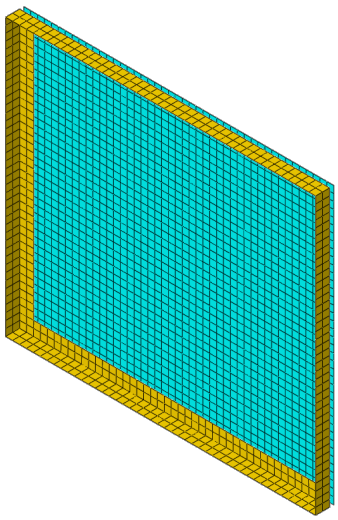

Figure 3-6. Geometry and mesh for thermal model of 0.56 m wide by 0.50 m high window exposed to a propane line fire burner

Figure 3-7 shows the comparison of predicted temperature response of the window at the exposed surface, mid-depth, and unexposed surface to experimental results for the 14 kW/m^2 (1.23 Btu/s-ft^2) and 27 kW/m^2 (2.38 Btu/s-ft^2) exposures. Experimental temperature data was only recorded at the time of significant events so only a limited number of data points was available for each location during each exposure. Measured mid-depth temperatures were lower than predicted, which is likely due to the thermocouple feeding directly from the back of the window to the mid-depth location. Since the thermocouple is not in the plane of measurement for 25–50 mm (1.0–2.0 in.), the measured temperature will be lower than the mid-depth temperature due to heat losses along the thermocouple.

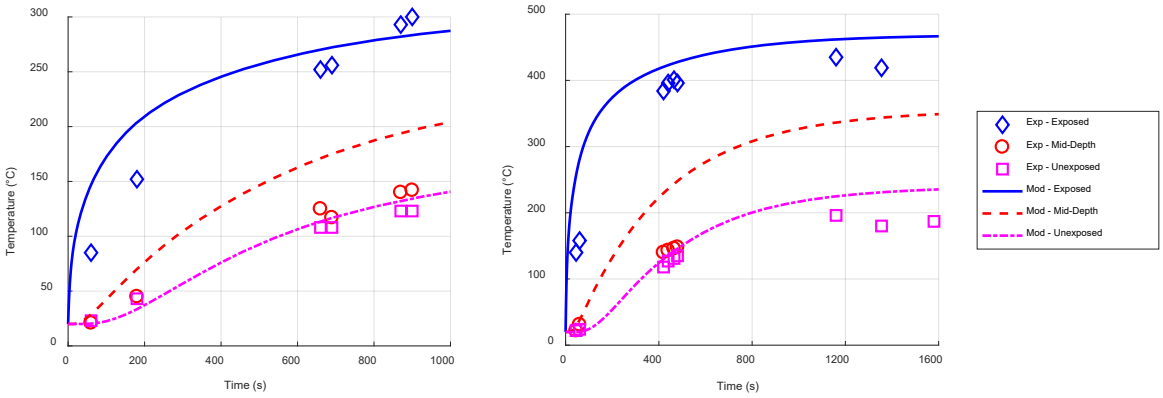

Figure 3-7. Predicted thermal response of polycarbonate windows compared to measurements by Strege et al. [10] for (left) 14 kW/m^2 and (right) 27 kW/m^2 exposures

The thermal model results were then used as input into the mechanical model. The mechanical model included just the polycarbonate window and made use of the vertical symmetry plane at the window center. Like the thermal models, the window was modeled with two-dimensional shell elements with nine section points through the thickness. Models of the smaller windows were meshed with in-plane mesh size of 12.7 mm (0.5 in). Meshes in the larger window models were refined to smaller sizes in areas of high strain based on initial modeling with mesh sizes ranging from 7 mm (0.28 in) to 23 mm (0.91 in). The larger window model mesh is provided in Figure 3-8. The mechanical models used temperature dependent thermal properties including elasticity and plasticity obtained from Srivastava et al. (2010), thermal expansion, and creep from Caplan (1982) and the calibration tests performed during this work.

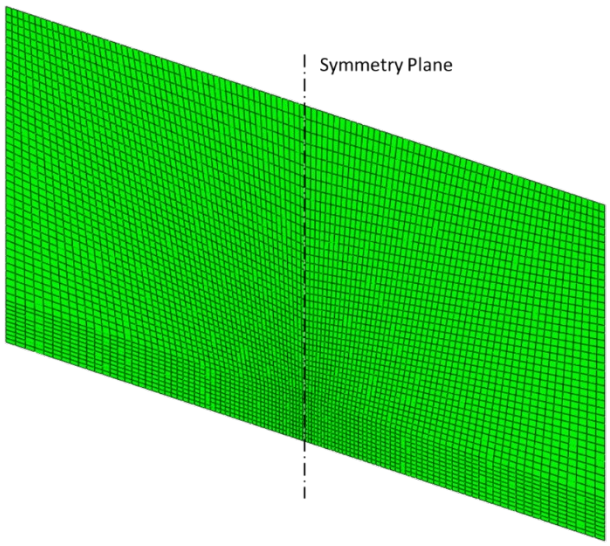

Figure 3-8. Mechanical model mesh for 1.42 m wide by 0.60 m high window model. Note only right half of window actually analyzed with assumed symmetry plane

The strain and deflection profiles at the time of window failure are shown in Figure 3-9 for the two sizes of windows tested by Strege et al. The locations of high strain and difference in deflections highlight the different failure mechanisms occurring in these two size windows shown in Figure 3-9. The smaller windows were predicted to undergo much less creep strains and less deformation than the larger windows. This means the smaller windows withstand higher temperatures and failure occurs when the unexposed surface temperature reaches 205 °C (401 °F), which is near the melting temperature of 225 °C (437 °F). The larger window buckles near the bottom of the frame generating tensile stresses in the upper portion of the window. These tensile stresses generate higher creep strains and cause failure of the window at a lower unexposed surface temperature of 188 °C (370 °F).

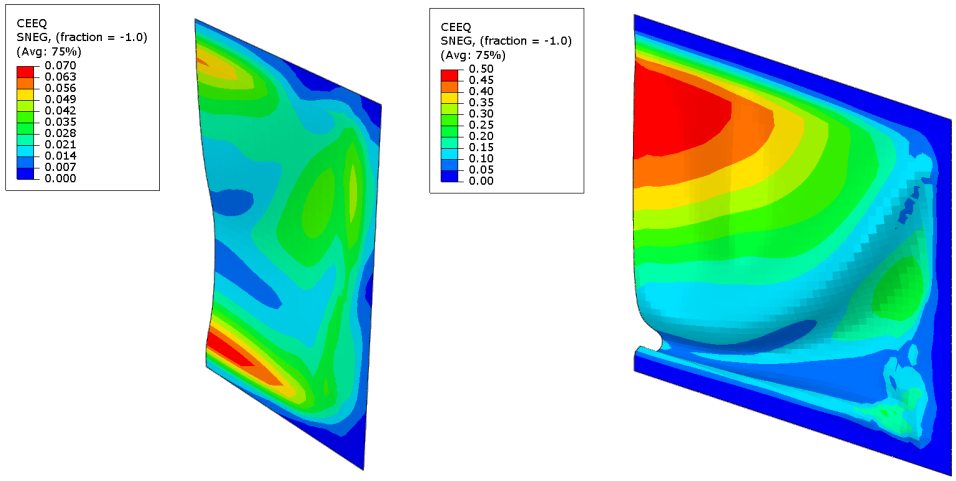

Figure 3-9. Equivalent creep strain profiles on displaced shape at predicted rupture time for (left) 0.56 m wide by 0.50 m high and (right) 1.42 m wide by 0.60 m high windows

The displayed profiles shown in Figure 3-9 are only the right half of window geometry. Table 3-2 shows a comparison of window failure times for each of the propane line burner tests conducted by Strege et al. The model predicts the correct trends in the data but consistently under-predicts rupture time of the window compared to experimental observation for the smaller window dimensions. The decrease in rupture time of larger windows is captured in the model although not to the extent as experimentally observed. One possible cause for these discrepancies is the movement and loss of material from the exposed surface of the window prior to failure. Melting and dripping of the exposed surface was observed during the experiments. While melting was also predicted in the model, the loss of material through dripping could not be included using current modeling techniques.

Table 3-2. Comparison of experimentally measured and numerically predicted window failure times for full scale polycarbonate windows

Dimensions, WxH (m)	Nominal Heat Flux (kW/m^2)	Time to Rupture (mm:ss)	
		Experiment	Model
0.56 x 0.50	14	>30:00	26:34
0.56 x 0.50	16	>30:00	21:57
0.56 x 0.50	27	19:20	12:42
0.56 x 0.50	40	12:15	10:26
0.56 x 0.50	80	8:45	7:02
1.42 x 0.60	40	6:24	8:45

3.5 Burn through Scaling Laws and Failure Criteria

The validated FE model of the windows was used to numerically explore the effects of physical scaling on the predicted failure time. The two window geometries used in the validation were considered to represent full-scale windows at two scaling ratios of 1:2 (one-half) and 1:5 (one-fifth). The width of the windows were scaled by these ratios while the heights of the windows were scaled according to the compartment fire model scaling method presented in Section 2.2. Window height were scaled according to the compartment fire model opening scaling laws so that airflow into the rail car is correct after the windows fail. The full and reduced scale window dimensions considered here are provided in Table 3-3. Initial scaling models were conducted with a 40 kW/m^2 (3.52 $Btu/s\text{-}ft^2$) exposure and maintained a window thickness of 12.7 mm (0.5 in.) so that thickness scaling could be used to develop consistent window failure times across all physical scales.

Table 3-3. Window dimensions considered for investigation of physical scaling

Scale	Type A Window		Type B Window	
	Width (m)	Height (m)	Width (m)	Height (m)
Full (1:1)	0.56	0.5	1.42	0.6
1:2	0.28	0.315	0.71	0.378
1:5	0.112	0.171	0.284	0.205

Table 3-4 provides predicted window rupture times at the reduced scales. For the small window (Type A), the rupture time is insensitive to the reduction in window size. This is because the deformation profile, and subsequent stress profile, of the window that drives the rupture mechanism is unchanged as the window scale is decreased. For the Type B window, when the size of the window is reduced the failure mechanism changes to be similar to a smaller size window (i.e., Type A) resulting in failure times and temperatures similar to Type A windows. Therefore, an increase in rupture time is seen when comparing the 1:1 scale with the 1:2 scale, but when comparing the 1:2 scale with the 1:5 scale no additional increase in rupture time is observed. This means that if a window is large enough, a thickness scaling rule must be applied for reduced-scale windows to match the full-scale window rupture time, but below a particular size no thickness scaling is necessary. The size of the window where thickness change affects the failure time was not fully resolved in this study. The effect of thickness scaling on the larger window is seen in Figure 3-10 for the 1:2 scale of a Type B window. With a full-scale predicted rupture time of 525 seconds, a thickness reduction from 12.7 mm (0.50 in) to 11.75 mm (0.46 in) is necessary to replicate the rupture time at 1:2 scale. While this thickness scaling can produce theoretically identical rupture times, available thicknesses for testing are often limited by manufactured availability. Obtaining the thickness needed to match full-scale rupture times will likely not be possible if readily available materials are to be used in testing. For example, polycarbonate material may only be available in 12.7 mm (0.50 in) and 11.1 mm (0.4375 in) thicknesses. Thus, possible rupture times for the reduced scale Type B windows would be 604 seconds and 475 seconds when the desired rupture time to match full-scale behavior is 525 seconds. Nonetheless, the model can now be used to determine the scaled window size that would produce a similar failure time for use in reduced scale experiments.

Table 3-4. Window failure conditions for different sized windows exposed to 40 kW/m^2 heat flux

Window Type	Scale	Failure Time (mm:ss)	Backside Temperature (°C)
A	1:1	10:26	205
	1:2	10:27	205
	1:5	10:29	204
B	1:1	8:45	188
	1:2	10:04	205
	1:5	10:04	205

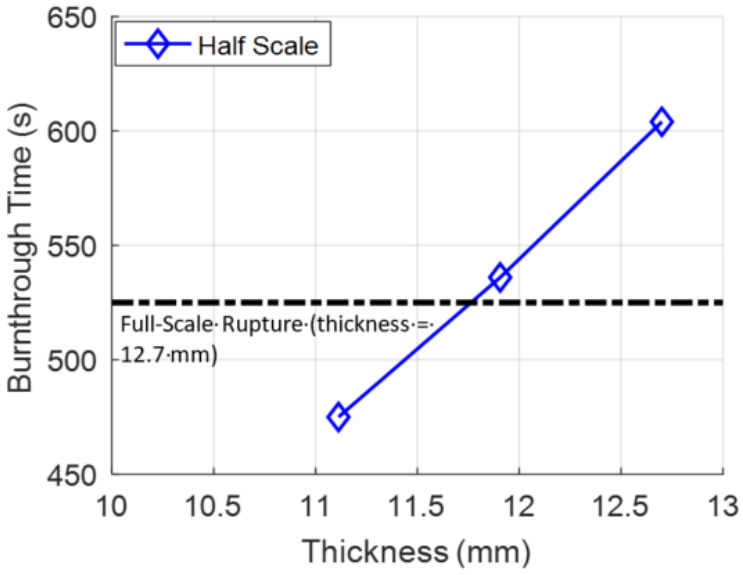

Figure 3-10. Effects of thickness scaling on 1:2 scale Type B window

3.6 Section Summary

Fire-induced rupture of polycarbonate windows affects the HRR of a burning rail car through the introduction of additional vent paths of the rail car interior. The window failure rupture time can be predicted for a variety of window geometries and fire exposures using a multi-mechanism model that includes the effects of window melting and high-temperature creep rupture. Mechanical creep testing of polycarbonate above the glass transition temperature (~165 °C [329 °F]) was combined with literature data to calibrate the multi-mechanism model. Rupture predictions using the model were generally within 30 percent of existing experimental temperatures and rupture times. This is excellent agreement for high temperature failure due to creep rupture where agreement to within an order of magnitude is regarded as acceptable.

Reductions in window sizes causes an increase in predicted rupture time only if the window is of sufficient size. Larger windows were observed and predicted to undergo a different deformation and stress evolution causing failure at lower window temperatures. For these larger windows (1.5 m wide by 0.5 m high [4.92 ft. x 1.64 ft.]), reductions in the window thickness can offset the effects of the different stress evolutions at smaller scales resulting in equivalent rupture time at smaller scales. However, the rupture time is sensitive to window thickness and the availability of standard thickness increments can limit the ability to accurately reproduce full-scale window rupture times at reduced scale. For smaller windows (0.5 m wide by 0.5 m wide [1.64 ft. x 1.64 ft.]), the predicted rupture time is relatively insensitive to the window size so in-plane scaling can be implemented with no thickness scaling to maintain window rupture time.

4. Fully-Developed Fire Simulations using FDS

Developing appropriate modeling methods to predict the HRR time history of a rail car fire is needed so that designers and operators can evaluate equipment and refine designs to improve safety. Methods for using the detailed computational model FDS to model the HRR time history of a rail car fire were explored in this initial research. Specifically, the research focused on the type of sub-model to be used in FDS to predict the material burning behavior. This model was evaluated since it can capture the spatial and time variations in the fire conditions which can affect the material burning behavior.

4.1 Background and Previous Work

For fire in complex geometries, it is difficult to estimate its HRR and flame spread through hand calculations or empirical models. Consequently, detailed CFD models have been used to study the fires within the rail cars in the past [18]–[22]. Some of the modeling efforts were performed to investigate the effects of ventilation and traveling fires on the predicted HRR with a simplistic fuel loading for the rail car [20] [23]. Peak HRRs were predicted to range from 6.5–39 MW (6,161–36,965 Btu/s) for the rail car, but no model validation was presented. A follow-on computational study evaluated the impact of rail car layout differences on the fire development inside of a rail car [21]. These modeling results determined that fire growth was slower in first class intercity rail cars compared with coach class rail cars due to the seats being closer together in the coach-class cars allowing the fire to more readily spread along on the rail car.

In a separate study using FDS [19], the researchers investigated different methods for modeling the burning behavior of fuels. This study was conducted on a 23.0 m long, 3.4 m high, 3.0 m wide (75.4 feet long, 11.1 feet high, 9.8 feet wide) rail car with 18 double pane glass windows 1.9 m wide and 0.6 m high (6.2 feet wide and 2 feet high). The fire scenario had two side doors open (each door is 0.9 m wide and 2.6 m high [3 feet wide and 8.5 feet high]) and the initiating fire 50 kW (47 Btu/s) for 2 minutes and 150 kW (142 Btu/s) for 8 minutes, European Norm (EN) 45545-1 arson scenario) at one end of the rail car in a corner. Glass windows were assumed to fail when they reached a critical temperature of 600 °C. The HRRPUA model FDS simulation provided a peak HRR 25 percent higher than the measured HRR in the large-scale test [24] (see Figure 4-1), and the predicted fire growth to the peak was faster than measured in the testing. This may be attributed to the window failure temperature criteria used or not including the effects of local oxygen concentrations on burning rate. A second simulation was performed using the pyrolysis model in FDS to predict material burning, which requires more detailed input data. This model produced a similar HRR time history compared with the large-scale test, except the peak between 1,000–1,500 seconds was under predicted by 35 percent and less pronounced. This is possibly due to not accurately predicting window failure times. The burning area base calculation in Figure 4-1 uses the summation method with cone calorimeter data [25] with the spread rate along the rail car taken from the large-scale test temperature data. This over-estimation of the measured HRR is likely due to not accounting for the effects of the fire dynamics on spatial variations in oxygen concentration and gas temperature, which would affect the exposure for the material burning.

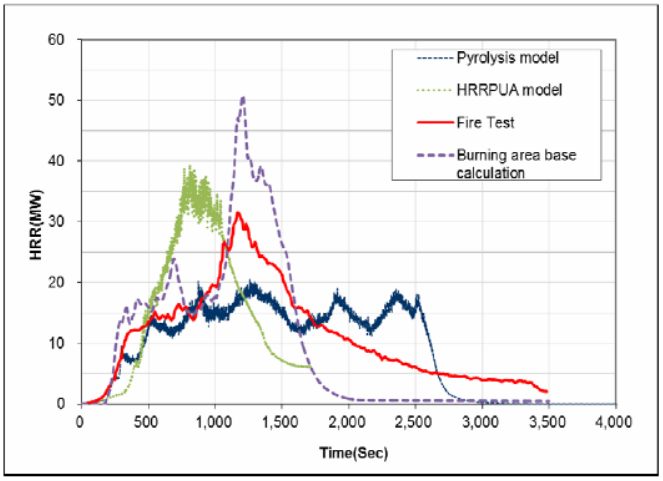

Figure 4-1. Heat release rate predicted using FDS, Version 5 with different material burning models compared with large scale experiments [19]

In general, the fully-developed fire modeling results from FDS appear to be promising since the model can capture the physics of the traveling fire phenomena [26], which is difficult to predict using other models. All the previous studies using FDS were performed using Versions 4 and 5 of FDS, which are outdated compared to the current Version 6. This is notable since significant changes were made in FDS from Version 5 to 6, particularly in the turbulence modeling which can have a significant impact on the predicted gas temperatures. Results are expected to be better using the more recent version of FDS. Moreover, during flame spread, the heat flux experienced by the solid material surface should presumably vary instead of staying at a fixed value. This possible situation brings great difficulty for using the HRRPUA model, which directly assigns a HRRPUA curves measured using a constant heat flux cone calorimeter test on the material. Such an approach could cause error in the prediction of the HRR for a fully-developed rail car fire due the variation in the exposure from low oxygen concentrations and spatial variations. A more sophisticated pyrolysis model will naturally account for the fluctuation in exposure at the surface, and it is expected to result in a more accurate prediction of the overall HRR. Therefore, a study was performed to evaluate these two approaches for predicting the HRRs of fully-developed fires using the newest version of FDS and determine the most appropriate modeling technique to use for rail car applications.

4.2 FDS Fully-Developed Fire Validation

FDS was selected to simulate the fully-developed fire within rail cars to account for the spatial and time varying conditions inside of a rail car. Before performing FDS simulations on a rail car, it was necessary to validate FDS for predicting the occurrence of flashover and fully-developed fire conditions. The model was validated against the experiment data reported in Bullen et al. [27]. In this study, fires tests were conducted using industrial grade of ethanol (IMS) as well as solid PMMA plastic sheet. Fires were burned in the open and in the center of a 2.0 m wide, 1.0 m high, 1.0 m deep (6.55 ft. x 3.28 ft. x 3.28 ft.) compartment. The material and burning properties of IMS and PMMA were taken from the Society of Fire Protection Engineers (SFPE) Handbook. The mass loss rates (MLR) of the fires simulated were then compared to the experiment data from Bullen et al. (1979) to validate that FDS captured the compartment fire behavior. Two different rectangular ventilation opening factors ($AH^{1/2}$) of 0.25 and 0.5 were

simulated to provide air flow into the compartment, where A is the opening area and H is the height of the opening in meters. In addition, two different pool fire areas (0.186 and 0.372 m^2 [2.0 and 4.0 ft^2]) were also simulated. The burning of the fuel materials was initiated by applying a 100 kW/m^2 (8.8 Btu/s-ft^2) exposure to the fuel surface for a short period of time (30 seconds). Figure 4-2 shows the setup of the simulation and flames generated by the fire.

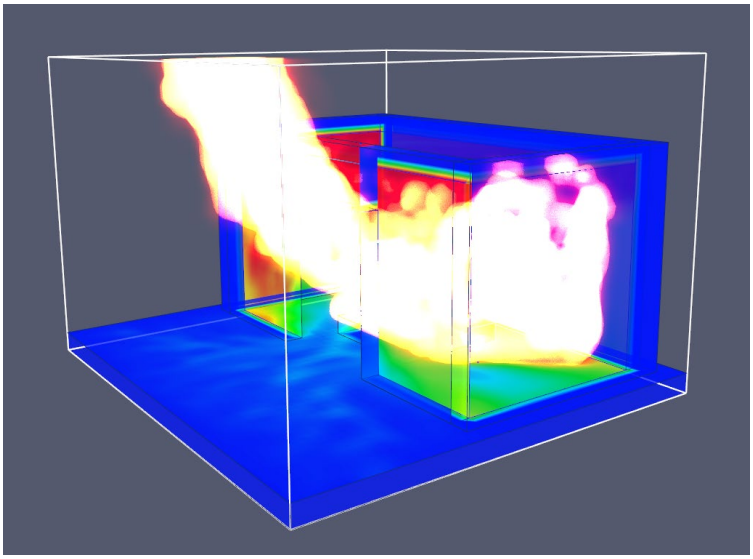

Figure 4-2. FDS validation simulation setup and flame generated by the pool fire

The post-flashover MLRs from the FDS pyrolysis model simulations are compared with the measured values in Table 4-1. The MLR results obtained from the simulations show good agreement with the experimental data with FDS to predict the MLR within 25 percent. In addition to being able to predict reasonable MLR, the FDS model was also able to distinguish whether a compartment would reach flashover or remain in a pre-flashover stage, which is important in simulating fully-developed rail car fires.

Table 4-1. Validation of FDS fully-developed compartment fire model

Fuel Type	Door Ventilation Opening Factor $AH^{1/2}$	Fuel Area 0.186 m^2			Fuel Area 0.372 m^2		
		Exp MLR (g/s)	FDS MLR (g/s)	Deviation	Exp MLR (g/s)	FDS MLR (g/s)	Deviation
PMMA	0.25	12	15	25.0 percent	21	19.7	6.2 percent
	0.5	No Flashover	No Flashover	0.0 percent	31	30.6	1.3 percent
Ethanol (IMS)	0.25	19	19.7	3.7 percent	30	28.8	4.0 percent
	0.5	26	32	23.1 percent	42	48.8	16.2 percent

4.3 Material Property Determination for FDS Model

To accurately predict the solid material behavior in a fire, the decomposition kinetic parameters and thermal properties of the solid materials must be either measured from experiments or

estimated through optimization. Past studies have shown the effectiveness of using optimization methods for determining the properties of solid materials [28] [29]. In this optimization technique, properties of the material are varied and then run through the burning model until there is agreement between the model and the data. In this study, properties for nine different materials commonly used in a rail car were determined using the optimization method. Table 4-2 lists the materials and their physical descriptions. A Shuffled Complex Evolution (SCE) algorithm along with the FDS model was used together to perform the optimization.

Table 4-2. Rail car materials that properties were determined using optimization method.

Material	Description and End-Use
Sample 1	Opaque thermoplastic material, nominally 3.81 mm (0.150 in.) thick, used for seat backs, wall panels, window masks, partitions, and ceiling panels
Sample 2	Composite material consisting of a layer of plywood sandwiched between layers of aluminum, nominally 12.7 mm (0.500 in.) thick, used for wall panels, ceiling panels, and closets
Sample 3	Composite material consisting of a layer of balsa wood sandwiched between layers of aluminum, nominally 15.9 mm (0.625 in.) thick, used for wall panels, ceiling panels, and closets
Sample 4	Translucent thermoplastic material 4.5 mm (0.177 in.) thick, used for light fixtures
Sample 5	Opaque thermoplastic material, nominally 4.75 mm (0.187 in.) thick, used for seat backs, wall panels, window masks, partitions, and ceiling panels
Sample 6	Fiberglass material, nominally 7.0 mm (0.275 in.) thick, used for wall lining, window masks, and seat components
Sample 7	Fiberglass material, nominally 3.27 mm (0.128 in.) thick, used for wall lining
Sample 8	Seat cover material, used for seat composite
Sample 9	Seat foam material, used for seat composite

The general procedure of determination of the material properties is as follows:

1. Conduct Thermogravimetric Analyzer (TGA) experiments at three heating rates (5, 10, 20 K/min) and determine kinetic parameters
2. Conduct three ASTM E1354 cone calorimeter tests each at a different exposure (25 or 35 depending on ignitability, 50 and 75 kW/m^2)
3. Use the SCE optimization algorithm and mass loss from two cone calorimeter tests at different exposure levels as well as the kinetic parameters obtained from TGA tests to determine the material properties of the samples
4. Validate the parameters with the remaining cone calorimeter data

The TGA tests on samples were performed using a TA Instruments Discovery Series TGA550 apparatus using aluminum cups in a nitrogen environment with a temperature range of 20 °C to 600 °C (68 °F to 1,112 °F). The bench-scale fire tests of materials were performed in an ASTM

E1354 cone calorimeter apparatus [31] and were used for estimating and validating the solid material properties as reported in previous report [30].

The determined material properties were then implemented into a gas phase FDS simulation of the cone calorimeter to fully demonstrate the predictive capability. Results of the cone calorimeter simulation were validated against the experimental results and corresponding HRRPUA model prediction. Figure 4-3 contains the comparison of the HRR obtained from experiments, gas phased simulation using the pyrolysis model, and HRRPUA model for Sample 1 at a 50 kW/m^2 (4.4 Btu/s-ft^2) exposure. A comparison for Sample 5 is provided in Figure 4-4. It was observed that the pyrolysis model with optimized material properties predicts the HRR from a sample within 25 percent. The pyrolysis model generally under-predicted the HRR compared to the experimental data. This was attributed in part due to the accuracy of the predicted flame radiation back to the fuel surface. As expected, the HRRPUA model predicts the curve at the provided heat flux well since this is the model input. If the heat flux is changed, the HRRPUA prediction would have significant error. The other validation cases are provided in Appendix A.

The pyrolysis model predicted time to ignition when an ignitable mixture was present in the gas phase. Using this approach, the pyrolysis model generally predicted shorter times to ignition compared with data. This may be due to the presence of fire retardant additives or some initial mass loss being non-combustible. The HRRPUA predicted ignition time using a transient heat conduction algorithm using the determined material properties and an experimentally measured ignition temperature. Using this approach, the HRRPUA model did provide accurate prediction of the time to ignition. Overall, both approaches provided reasonable predictions of ignition time.

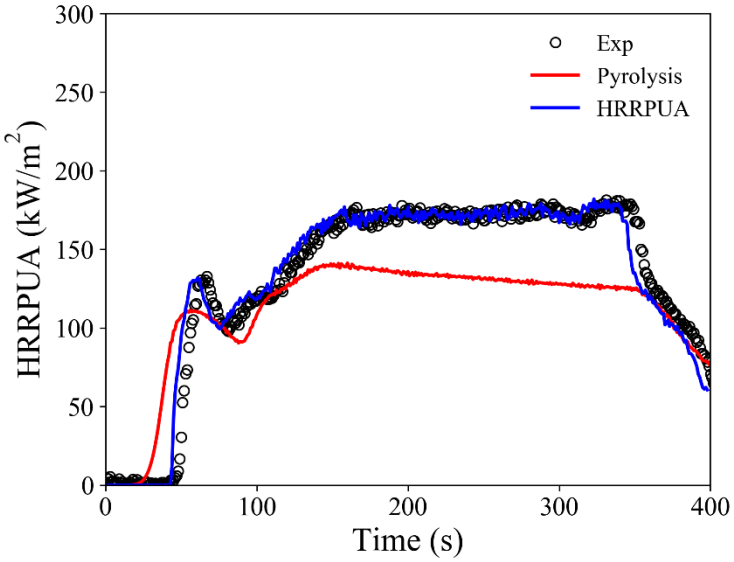

Figure 4-3. Validation of HRRPUA obtained using optimized material properties for Sample 1

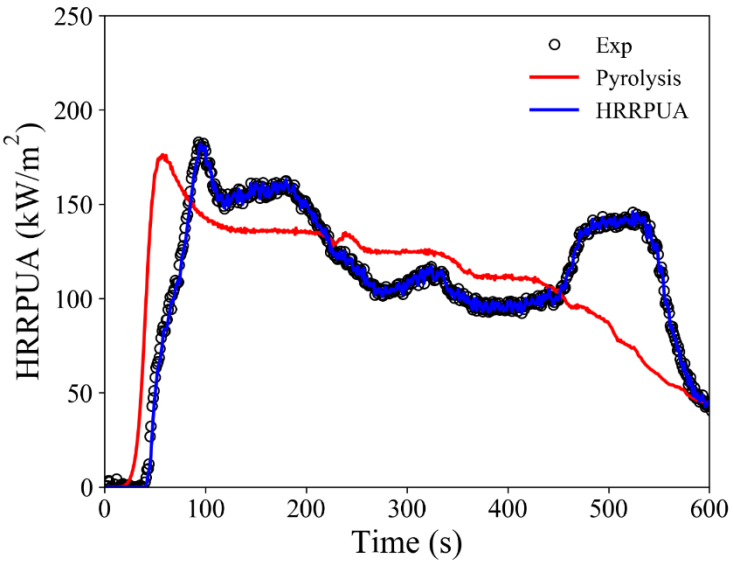

Figure 4-4. Validation of HRRPUA obtained using optimized material properties for Sample 5

4.4 FDS Full Rail Car Simulation

Rail car simulations were conducted on an exemplar rail car 23.2 m long, 2.75 m high, and 3.2 m wide (76.0 ft long, 9.0 ft high, and 10.5 ft wide) with four side doors 2.0 m high, and 1.25 m wide (two on each side). A series of 30 polycarbonate windows were distributed along both sides of the rail car with 24 windows being 0.6 m x 0.6 m (2.0 ft x 2.0 ft) and 6 windows being 1.5 m wide and 0.6 m high (4.9 ft wide and 3 ft high). Both the HRRPUA and pyrolysis model were used in this effort to predict the development of a fire inside of a rail car including the growth, occurrence of flashover, fully-developed stage, and decay. The most significant difference between these two models is how the material mass loss rate and HRR are determined. For the HRRPUA model, material burning is predicted using a HRRPUA curve measured at a reference heat flux (e.g., 50 kW/m^2 [4.4 Btu/s-ft^2]) in the cone calorimeter. However, the HRRPUA model assumes the solid surface will be exposed to a constant heat exposure during entire burning duration. Such an assumption may not always be true since the thermal exposure experienced by a solid surface typically fluctuates, especially for a fully-developed fire where the exposure is a function of time, amount of burning fuel, and ventilation. Therefore, the HRRPUA model will have more error when the thermal exposure is more variable. The pyrolysis model uses the predicted thermal exposure to predict the mass loss rate and HRR of the material. With this approach, the effects of locally low oxygen concentrations and spatial variations in exposures can be accurately accounted for in the simulation.

A comparison of the predictions from FDS models with the two different types of burning algorithms was evaluated using an exemplar rail car. Figure 4-5 shows the setup of the model. A 300 kW (284 Btu/s) propane burner was placed at the left corner of the rail car as the initiating fire and is marked as red in the figure. Table 4-3 includes a list of materials used in the rail car simulations. For the HRRPUA model, the thermal properties obtained from the optimization are used for the solid surface. Two different HRRPUA reference curves (exposure of 50 and 75 kW/m^2 [4.4 and 6.6 Btu/s-ft^2]) were evaluated in the simulations to assess the effect of different

HRRPUA curves on the results. A mesh size of 0.05 m (2.0 in) was used with a total of 897,608 computational cells. Windows were taken to be noncombustible in this simulation and were predicted to fail creating an airflow path when the unexposed side temperature of the window reached 205 °C (401 °F).

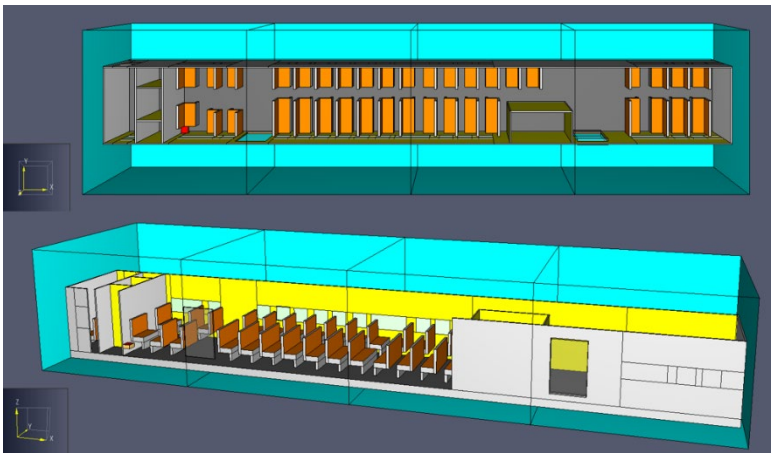

Figure 4-5. A full rail car simulation model

Table 4-3. Materials used in the rail car model

Surfaces	Materials Used
Side walls	Sample #1, yellow color surface
End walls	Sample #2, light grey color surface
Ceiling	Sample #5, green color surface, not show in Figure
Floor	Sample #6, dark grey color surface
Seats	Sample #9, orange color surface

Figure 4-6 includes a plot of the HRR of a full rail car fire obtained from pyrolysis, 50 kW/m^2 (4.4 Btu/s-ft^2) HRRPUA and 75 kW/m^2 (6.6 Btu/s-ft^2) HRRPUA models. It was observed that the 75 kW/m^2 (6.6 Btu/s-ft^2) HRRPUA model had the highest peak HRR and fastest growth of fire among the three models. The HRR of the fire sharply increased around 250 seconds until it reached its peak of 40 MW (37,913 Btu/s) at approximately 400 seconds and then gradually decreased as the materials burned out. The HRR curve obtained using the 50 kW/m^2 (4.4 Btu/s-ft^2) HRRPUA model had a similar shape compared with the 75 kW/m^2 (6.6 Btu/s-ft^2) HRRPUA model but with a slightly lower peak HRR (~35 MW [33,174 Btu/s]) and slower growth rate. For the pyrolysis model, the HRR growth was similar to that predicted using the HRRPUA models up to 250 seconds and then decreased. After this point, the pyrolysis model predicted a steady increase in the HRR up to 1,000 seconds to a peak of 22 MW (20,852 Btu/s) after which the material burn out caused the HRR to steadily decrease.

This difference between HRRPUA and pyrolysis model was attributed to the limited air flow into the rail car through the openings. The development of the fire detailed below demonstrates highlights the differences between the HRRPUA and pyrolysis model predictions.

1. Before Point A in Figure 4-6, the materials near the initiating fire were ignited in both the pyrolysis and HRRPUA models. The fire then starts to spread toward the center of the rail car.
2. Between Points A and B, the pyrolysis model HRR decreased due to a decrease in oxygen concentration causing the exposure to decrease on materials in the center of the rail car. The HRRPUA models predict a continuous increase in HRR since the burning in these models are not affected by the change in exposure level. The pyrolysis model predicted HRR began to increase when materials at the door on the opposite end of the rail car ignited.
3. At Point C, the windows of the rail car started to break, which increased the airflow into the rail car. Due to the increase in oxygen, the gas temperature inside of the rail car increased causing the exposure to increase. For the HRRPUA models, the burning was unaffected by the local fire conditions and the continued to spread along the length of the rail car reaching its peak around Point C.
4. Between Points C and D, the windows progressive fell out along the length of the rail car and the HRR predicted by the pyrolysis model gradually increased. For the HRRPUA model, the intense burning associated with the rapid fire spread caused materials to begin burning out causing the fire to transition into the decay stage.
5. At Point D, all the windows failed. For the pyrolysis model, materials within the rail car model had started burning out causing the HRR to decrease. The HRRPUA model remained in the decay stage.

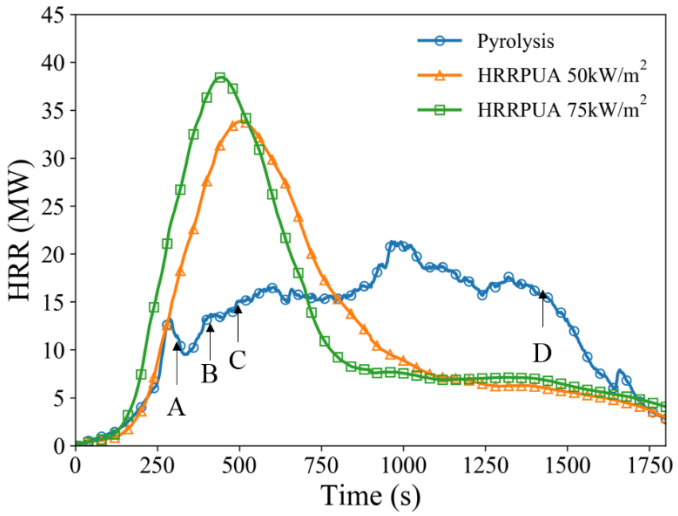

Figure 4-6. HRR of a rail car fire obtained from HRRPUA and pyrolysis FDS models

The different burning processes can also be seen through the plots of burning rates of solid surfaces within the rail car. Figure 4-7 contains snap shots of the burning at different times around the peak burning period for the simulation using the 50 kW/m^2 (4.4 Btu/s-ft^2) HRRPUA model. In this simulation, the flame was predicted to steadily spread from one end of the rail car to the other. A similar behavior was observed with the 75 kW/m^2 (6.6 Btu/s-ft^2) HRRPUA model simulation. For the simulation using the pyrolysis model, a different behavior was observed. Figure 4-8 includes a series of plots of material burning rates at different times of the

pyrolysis model simulation. The materials at the center of the rail car are burning at 300 seconds; however, the material burning rates at the center are significantly reduced by 400 seconds due a lack of oxygen and reduction in thermal exposure. This is balanced by the ignition of materials by the opening at the opposite end of the rail car. As the windows begin to fail between 500–1,500 seconds, material burning rates in the center of the rail car increase and the fire begins to spread again toward the opposite end of the rail car.

This process can be further illustrated by the oxygen fraction within the rail car as well as in Figure 4-9 for the pyrolysis model simulation. At 200–300 seconds, the oxygen supply within the rail car is sufficient to sustain the combustion of ignited materials, which produces a hot gas layer within the rail car. However, at 400 seconds, the oxygen concentration within the rail car decreases to less than 6 percent due to limited airflow, except near the openings where the majority of burning is occurring. As the windows fail, airflow into the rail car increases causing the oxygen concentrations to increase. This increases the exposure levels which causes the burning rates to increase and enhances flame spread.

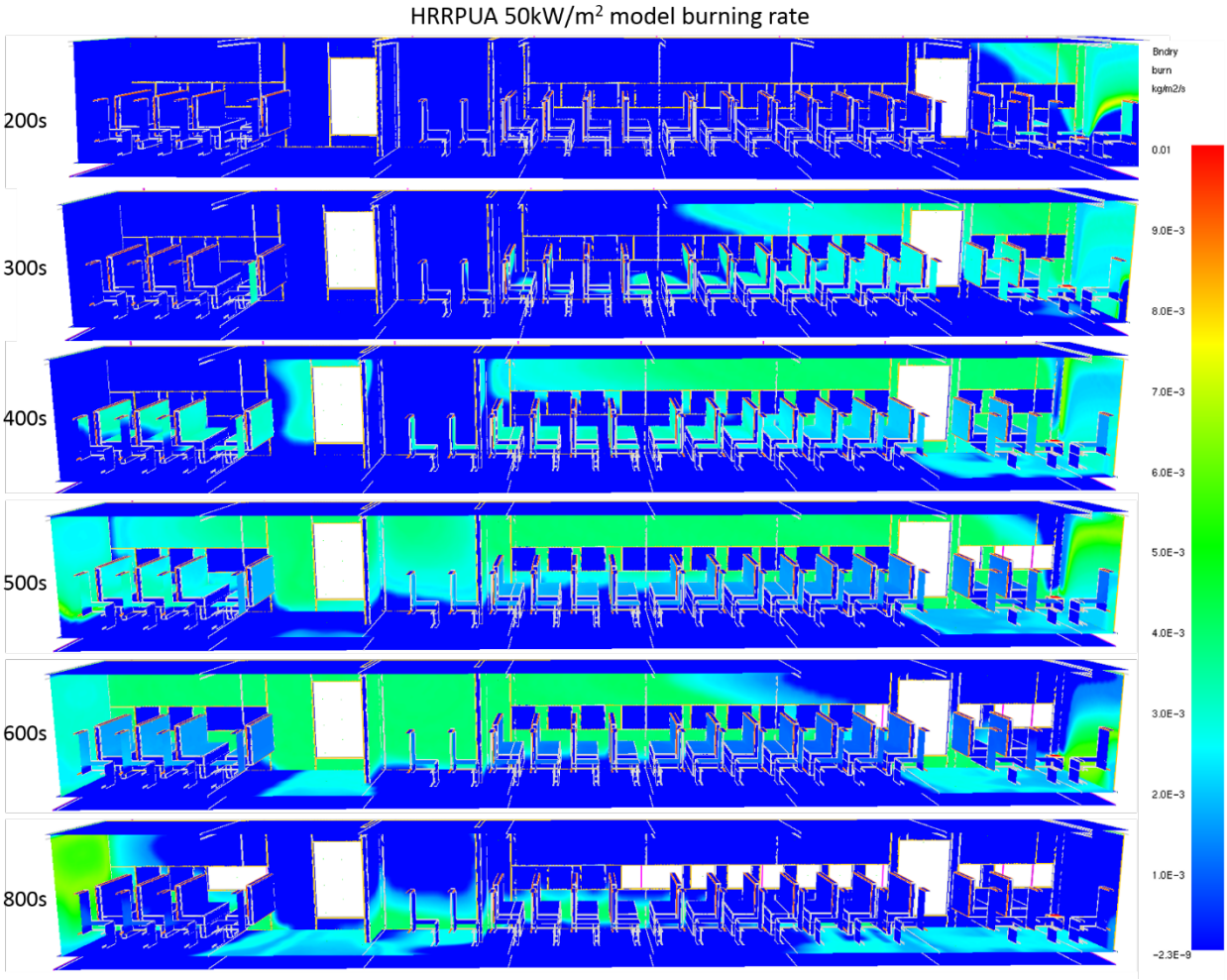

Figure 4-7. Burning rate of solid materials at various times using the 50 kW/m^2 HRRPUA model simulation

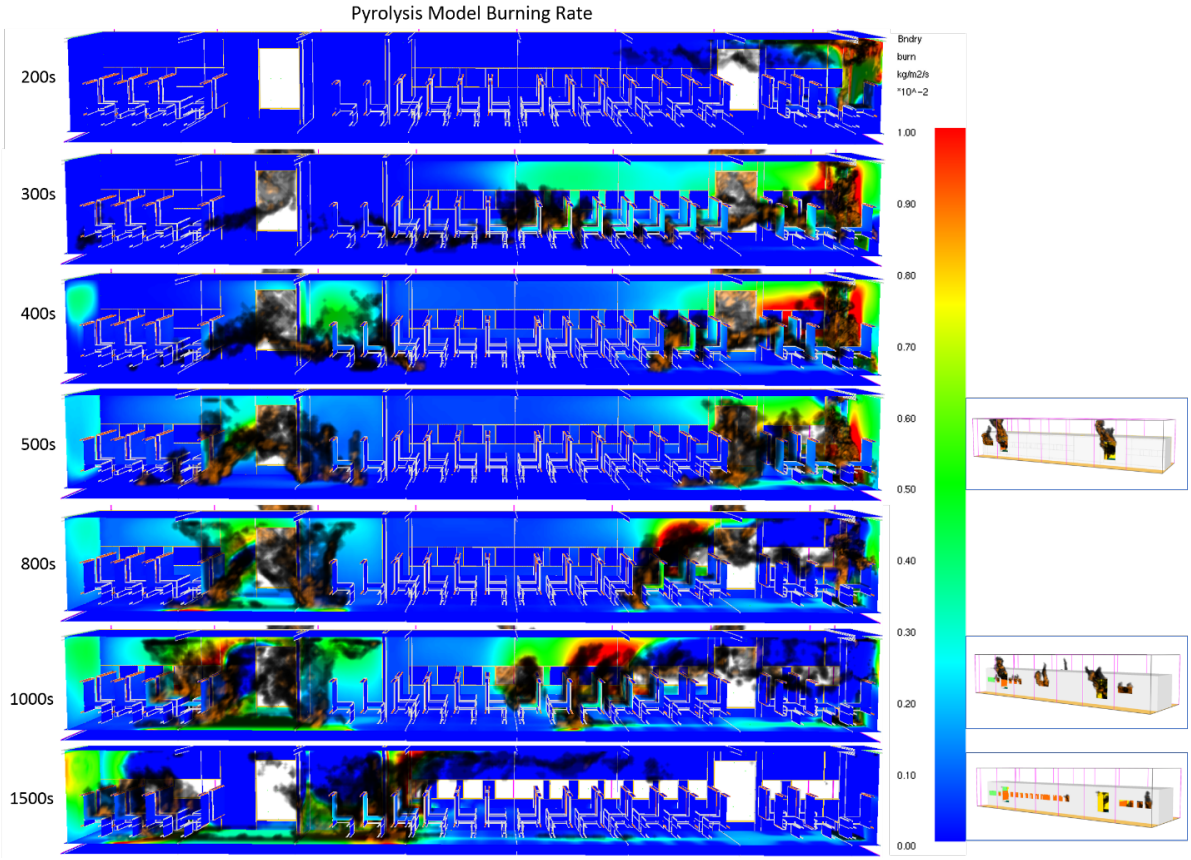

Figure 4-8. Burning rate of solid materials at various times using the pyrolysis model simulation

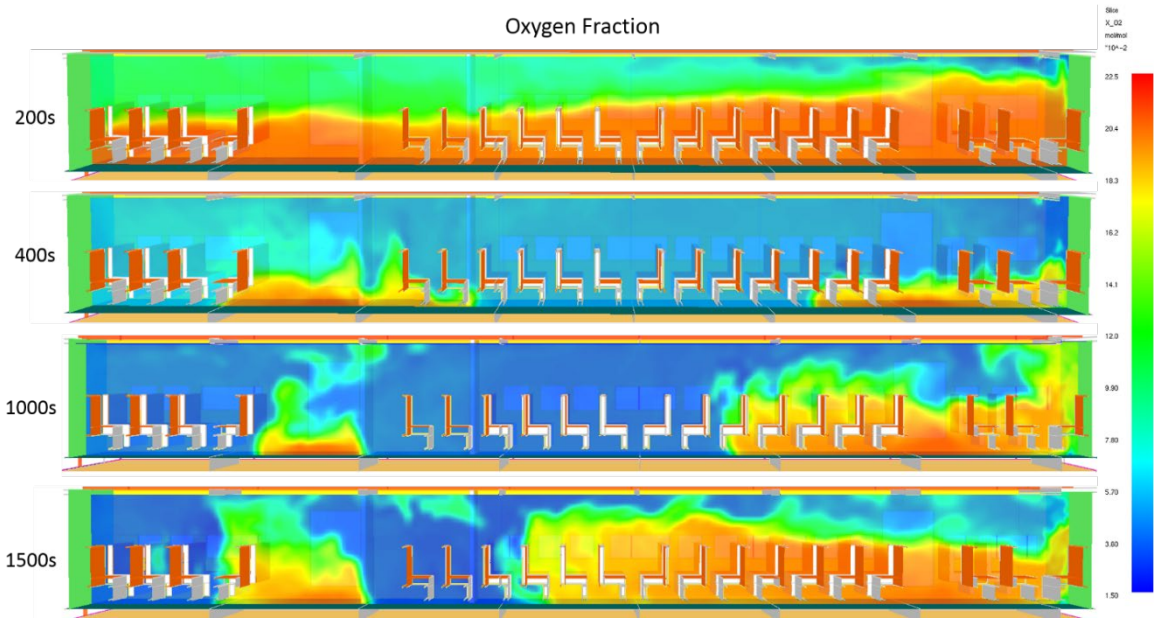

Figure 4-9. Oxygen volume fraction within the rail car at various times from pyrolysis model simulation

The difference in the burning processes of HRRPUA and pyrolysis models also affected the gas temperatures predicted within the rail car. The gas temperatures at four different locations 0.10 m (4.0 in.) below the ceiling shown in Figure 4-10 were monitored for all simulations. For the 50 kW/m^2 (4.4 Btu/s-ft^2) HRRPUA model simulation, the fire continuously spread along the length of the rail car due to the burning of material being dependent on its time to ignition. As seen in Figure 4-11a, the gas temperatures measured at Positions 1–4 sequentially increase above 600 °C (1,112 °F) before 500 seconds. Gas temperatures increased as the windows failed providing more air flow into the rail car allowing for more HRR inside of the rail car. All gas temperatures measured at the four different locations reached the peak temperature before 1,000 seconds. For the pyrolysis model, the gas temperatures are observed in Figure 4-11b to initially resemble those predicted using the HRRPUA model. However, as the oxygen concentration decreases and the material burning rates slow the gas temperatures rise more gradually compared with the HRRPUA model. Eventually, the materials at the end with the initiating fire near Position 1 begin to burn out causing the temperatures in this region to decrease below those in other areas. Gas temperatures at other areas peak around 1,500 seconds before decaying.

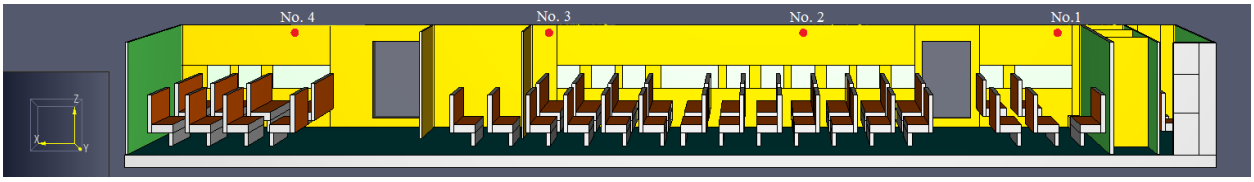

Figure 4-10. Temperature monitoring locations within the rail car model

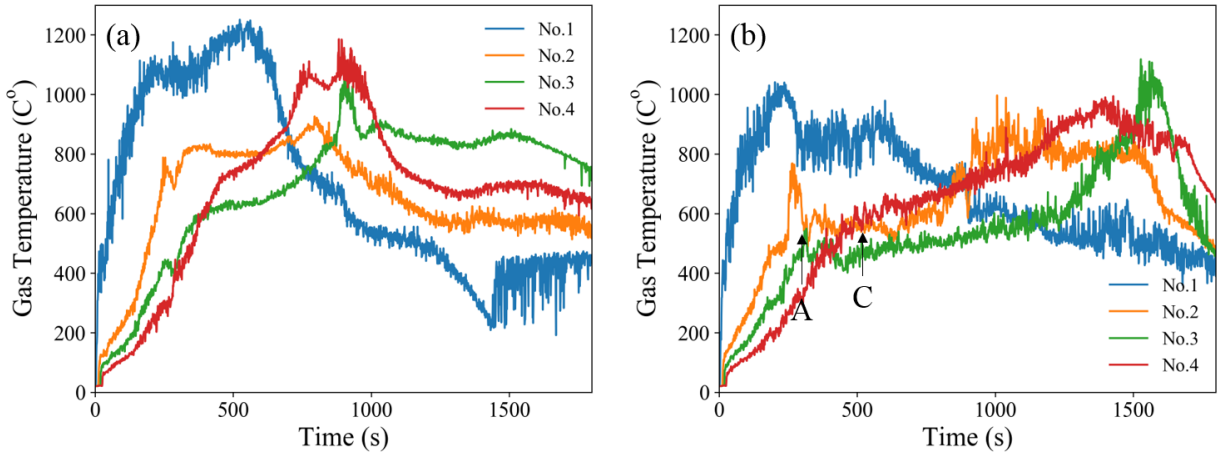

Figure 4-11. Gas temperatures measured at various locations within the rail car (a) 50 kW/m^2 HRRPUA model and (b) pyrolysis model

In general, the simulation results from the HRRPUA and pyrolysis models show a similar trend compared to the modeling and experimental results of Lee et al. (2013) (see Figure 4-1). For instance, the HRRPUA models in this study predict the same magnitude of peak HRR and faster increase of HRR compared to the pyrolysis model simulations. The HRR results obtained from the pyrolysis model in this study show a similar trend as the experimental data from Lee et al., i.e., fast initial growth, slowdown of growth, peak HRR at around 1,000 seconds, steady drop of HRR after the peak. More importantly, the simulation results from the pyrolysis models highlight that the material burning is affected by airflow into of the rail car through doors and

windows, which in turn affects oxygen concentrations and gas temperatures. The results also indicate that using the HRRPUA models may over-predict the rail car HRR due to the lack of feedback between the fire environment and the fuel burning rate. Therefore, it is recommended that FDS simulations using a pyrolysis model should be used to predict the HRR from a rail car.

4.5 Section Summary

It is difficult to predict the HRR history of a rail car fire (including fire growth, occurrence of flashover, fully-developed stage, and decay) due to geometry and variations in airflow into the rail car that affect the uniformity of the thermal exposure. To account for the geometric effects and airflow changes, CFD simulations were performed using FDS to predict the HRR history. FDS was validated with data and shown to be capable of predicting material burning rates within 25 percent of measured data and predicted the occurrence of flashover.

Two different material burning models were explored for use in the simulation study. The first model was a HRRPUA burning model where a reference HRR curve and ignition temperature are used to quantify the ignition and burning of materials. In the second model, a detailed pyrolysis model was used to predict material burning rate. Thermal and burning properties for the models were determined using an optimization method based on data from TGA and cone calorimeter experiments.

FDS simulations using the different burning models were used to predict the HRR history of an exemplar rail car. The pyrolysis model utilized the material properties determined from optimization method. FDS predictions were performed with two different HRRPUA reference curves (50 kW/m^2 and 75 kW/m^2 [4.4 $Btu/s\text{-}ft^2$ and 6.6 $Btu/s\text{-}ft^2$]) to quantify the impact on the results. The simulation results showed that the two HRRPUA models predict a faster growth rate to the peak HRR (400–500 seconds) compared to that predicted using the pyrolysis model (peak HRR at 1,000 seconds). This was demonstrated to be due to the fact that the pyrolysis model is affected by the changes in the local thermal exposure caused by changes in oxygen levels during the course of the fire, which is similar to what would occur in a real fire. Conversely, the HRRPUA model does not account for the effect of thermal exposure on burning rate resulting in a consistently spreading fire and earlier transition to fire decay. The trends in the results are similar to those quantified by Lee et al., but data on the materials inside the rail car prevented model validation with this data. Future experimental studies need to be performed to quantify the fire dynamics effects on the HRR history for rail cars.

5. Simple Model for Fully-Developed Fires

There is a need for a new simplified model to predict HRR which includes key physics (such as changing thermal exposure and ventilation) without detailed fire modeling for use by designers to assess tradeoffs to improve rail car fire performance. The following sections describe the development of a simplified model to meet this need.

5.1 Background and Previous Work

Several methods have been presented in the literature to predict the HRR of a fully-developed rail car fire. These models generally fall into three categories: average HRR methods, summation methods, and fire models. An overview of the current state of each of these methodologies was presented in [10]. Average HRR methods can be used to obtain a first estimate of peak HRR by calculating the total fuel load and estimating a burning duration [11]. However, these estimates generally under-predict the peak HRR due to averaging over the burning duration [10]. Summation methods use bench-scale cone calorimeter testing results to estimate the time resolved HRR for each component within the rail car. The overall HRR is predicted by summing the contribution of each material. The predictions of HRR are generally improved over average HRR methods; however, these methods do not account for changes in ventilation and are limited to fixed constant thermal exposure conditions [10]. A range of fire models have been used to predict the time-resolved HRR of a fully-developed rail car fire: semi-empirical models, single layer models, and detailed CFD models [10]. Fire models can provide detailed predictions of HRR, as discussed in the previous section; however, this type of approach requires an expert in fire protection for each analysis.

5.2 Description of Methods

The simple model developed in this work is an extension of the heat of gasification-based single layer fire model for rail cars presented in [12]–[15]. Note that this a single layer, well mixed model that does not resolve any spatial variations inside of the rail car. As a result, the location of the openings and fuels does not affect the model result. In this project, the single layer fire model is replaced with a semi-empirical relationship for gas temperature based on available ventilation. An overview of the fundamental basis of the methodology is provided in the following paragraphs.

The heat of gasification, ΔH_G, relates the thermal exposure, q''_{net}, to the mass flux of solid fuel decomposition and diffusion into the air, m'', through

$$q''_{net} = m'' \Delta H_G \tag{5-1}$$

The heat of combustion, ΔH_c, relates the HRRPUA, $\dot{Q}''$, to m'' by

$$\dot{Q}'' = m'' \Delta H_c \tag{5-2}$$

The HRRPUA can be related to the thermal exposure by equations 5-1 and 5-2

$$\dot{Q}'' = \left(\frac{\Delta H_c}{\Delta H_G}\right) q''_{net} \tag{5-3}$$

Researchers in [12]–[15] have calculated the net heat flux to combustible surfaces in a compartment using the equation

$$q''_{net} = \epsilon_s \sigma \left(\epsilon_g T_g^4 - T_p^4\right) + h\left(T_g - T_p\right) \tag{5-4}$$

where ϵ_s is the surface emissivity, ϵ_g is the gas emissivity, σ is the Stefan-Boltzmann constant, T_g is the exposure gas temperature, h is the convective heat transfer coefficient, and T_p is the pyrolysis temperature. The pyrolysis temperature for charring materials is estimated to be

$$T_p = T_g - 50 \tag{5-5}$$

the gas emissivity is estimated to be 0.9, and the surface emissivity is estimated to be 0.9 based on the values recommended by [12]–[15]. Using equations 5-3 through 5-5, the HRRPUA of each material can be calculated based solely on compartment gas temperature for fully-developed fires.

The previous work in the literature used a fire model to calculate the gas temperature; however, researchers have shown it is possible to relate the gas temperature of a fully-developed compartment fire to the available ventilation using an empirical relationship based on opening factor [4]. The opening factor, *OF*, can be calculated using the equation

$$OF = \frac{A_T}{A_w\sqrt{H}} \tag{5-6}$$

where A_T is the total solid surface area of the compartment including the floor, A_w is the total ventilation surface area, and H is the height of the ventilation opening. In the case of multiple ventilation openings, the $AH^{1/2}$ for the openings in the denominator of Equation 5-6 would be the sum of $AH^{1/2}$ of each individual opening. Physically this relates the total energy losses in the compartment to the maximum air available for combustion. Fully-developed fires with lower *OF* correspond to over-ventilated fires (fuel-limited) and higher *OF* correspond to under-ventilated (ventilation-limited) fires. The transition between over-ventilation and under-ventilation generally occurs between $10 \leq OF \leq 15$. Combining equations 5-4 to 5-6, the q''_{net} can be related directly to *OF*. For a specific fire scenario in a rail car, the opening factor can be calculated based on which doors and windows are open, and the impact of window failure can be considered by changing *OF* over time.

Experimental data relating opening factor, *OF*, to gas temperature, T_g, was only available up to a maximum *OF* 55; however, prior to window failure it is possible for the *OF* a rail car to be in the range of 40–1,000 based on the number of initially open doors and windows. Since the average gas temperature in heavily under-ventilated fires ($OF \geq 55$) are unlikely to reach flashover conditions as there is not sufficient oxygen available to sustain combustion, it is possible to use pre-flashover empirical relationships to predict the expected gas temperature, T_g.

Researchers showed that gas temperatures in pre-flashover compartments can be calculated using the equation

$$T_g = \mathrm{T}_\infty + 480\left(\frac{\dot{Q}}{1150A_w\sqrt{H}}\right)^{\frac{2}{3}}\left(\frac{h_k A_T}{3.8A_w\sqrt{H}}\right)^{-\frac{1}{3}} \tag{5-7}$$

where h_k is the effective heat transfer coefficient, and T_∞ is the ambient air temperature [16]. The maximum HRR inside a compartment which can be sustained based on available oxygen can be calculated by

$$\dot{Q}_{max} = 1500 A_w \sqrt{H} \tag{5-8}$$

combining equations 5-6 to 5-8 yields

$$T_g = T_\infty + 894 (h_k OF)^{-\frac{1}{3}} \tag{5-9}$$

typical values of h_k range from $0.001 - 0.1 \frac{kW}{m^2-K}$ (0.176–17.6 Btu/hr-ft^2-°F) for different materials. In this study $h_k = 0.055 \frac{kW}{m^2-K}$ (9.68 Btu/hr-ft^2-°F) (6 mm [0.25 in]) gypsum plaster [17] and $T_\infty = 20$ °C (68 °F) were used. The experimental data from [4] was used when $OF \leq 44$ and Equation 5-9 was used for $OF > 44$. The transition OF was selected based on the intersection of the two curves. The relationship between OF and T_g used in this work is shown in Figure 5-1.

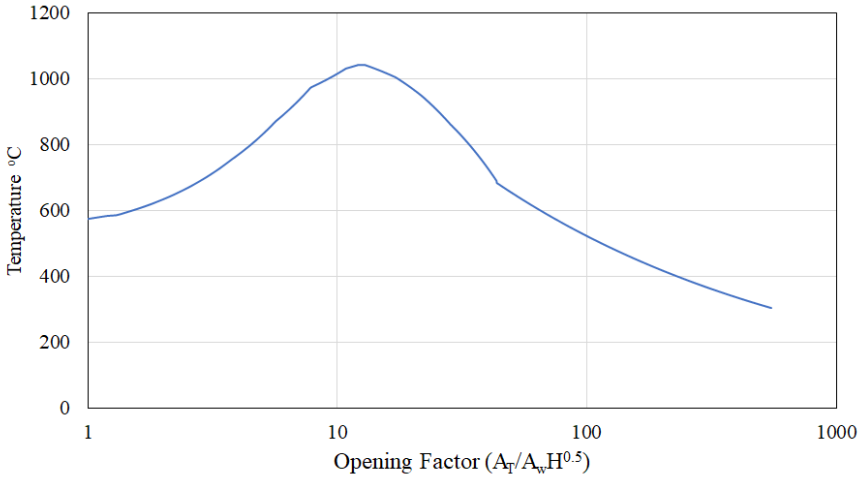

Figure 5-1. Relationship between compartment temperature and opening factor in fully-developed fires

It is important to account for the total energy available for combustion for each material to capture the impact of material burnout. The total energy load, E, for each material can be calculated based on the total mass, m, for each material using the equation

$$E = m \Delta H_c = \rho A \delta \Delta H_c \tag{5-10}$$

where ρ is the material density, A is the material surface area, and δ is the material thickness. The time-resolved HRR for each material can be calculated using the equation

$$\dot{Q}(t) = \min\left(\max\left(E - A \int_0^t \dot{Q}'' \, dt, 0\right), A\dot{Q}''\right) \tag{5-11}$$

where $\dot{Q}$ is the HRR, and t is the current time step. The overall HRR for the rail car is calculated by summing the time resolved HRR of each material.

5.3 Rail Car Description

Predictions with the simplified model were conducted using the rail car geometry and combustible interior finish previously used in the FDS modeling in Section 4. The total surface area, energy load, heat of combustion, and heat of gasification of each material in the rail car is summarized in Table 5-1. Four ventilation configurations were considered. In the first configuration, two doors on one side were open like the configuration used in the FDS simulations. A side single door was open in the second configuration, a single window was open in the third configuration, and four doors and six windows were open in the final configuration. In the first case like the FDS simulations in the previous section, the windows failed between 400–960 seconds. In the other cases, the ventilation remained constant at the initial ventilation condition (i.e., no other windows failed during the simulation). The initial opening factor for each configuration is summarized in Table 5-2. Note that this a single layer, well mixed model that does not resolve any spatial variations inside of the rail car. As a result, the location of the openings does not affect the model result.

Table 5-1. Summary of exposed materials in rail car

Surface	Material	$A\ (m^2)$	$\dot{Q}_{avg}$	$\Delta H_c\ (kJ/m^2)$	$\Delta H_g\ (kJ/kg)$	$E\ (MJ)$
Seat	Sample 9	104.65	70.9	50,690	3,888	3330
Flooring	Sample 6	73.18	101.6	19,380	1,037	7785
Exterior Walls	Sample 1	112.47	126.9	18,917	810	5603
Interior Walls	Sample 2	16.43	66.6	10,180	831	887
Ceiling	Sample 5	73.18	124.1	24,490	1,073	5575

Table 5-2. Initial ventilation configurations

Case ID	Initial Ventilation (width x height)	$A_w\sqrt{H}\ (m^{5/2})$	$A_T\ (m^2)$	$OF\ (m^{-1/2})$
1	2 doors (1.25 x 2.00 m)*	7.1	280.0	40
2	1 door (1.25 x 2.00 m)**	3.5	282.5	80
3	0 doors, 1 window** (1.20 x 0.60 m)	0.56	284.2	510
4	4 doors (1.25 x 2.00 m), 6 windows** (1.20 x 0.60 m)	17.6	270.6	16

*windows open between 400–960 seconds based on FDS simulations
**no other windows fail during simulation

5.4 Heat Release Rate Predictions

Predictions of the HRR of the railar in the first ventilation configuration using several methodologies is shown in Figure 5-2. In the fuel load method, the total energy of the rail car is divided evenly over an assumed 30-minute duration fire. In the HRRPUA method, the HRRPUA curves for each material from cone calorimeter testing at an exposure of 50 kW/m^2 (4.4 Btu/s-ft^2) are multiplied by the exposed areas. The total HRR of the rail car is then calculated by summing the HRR of each material. The Duggan method is similar to the HRRPUA method; however, HRRPUA curves from cone calorimeter experiments with different exposures are used depending on the position of the material in the rail car [18]. HRRPUA curves of the seats, flooring, and vertical walls used data from an exposure of 25–35 kW/m^2 (2.2-3.1 Btu/s-ft^2) and the ceiling used data from an exposure of 50 kW/m^2 (4.4 Btu/s-ft^2). The heat of gasification method used the simplified model presented in Section 5.2 of this report with an assumed t-squared growth to flashover and window failure times from the FDS modeling. The FDS HRRPUA and pyrolysis models are the methods presented in Section 4.4 of this report. Overall the HRRPUA, heat of gasification, and FDS HRRPUA model predict similar peak HRRs. Window failure between 400–960 seconds resulted in the peak HRR from the heat of gasification model increasing beyond the peak release rate from the HRRPUA model. This shows the predicted thermal exposure is higher than the 50 kW/m^2 (4.4 Btu/s-ft^2) exposure used in the cone calorimeter experiments. The heat of gasification approach predicts a higher HRR than the pyrolysis model due to the model not including the local fire effects on the burning as well as the spatial variations in the thermal exposure and burning.

Predictions of the HRR of the rail car in the second, third, and fourth ventilation configuration using the fuel load, HRRPUA, Duggan, and heat of gasification methods are shown in Figure 5-3, Figure 5-4, and Figure 5-5; respectively. These resutls highlight the benefit of the heat of gasification approach over other simplified models in predicting HRR for fully-developed fires. Since the gas temperatures in the heat of gasification approach are changed based on the available ventilation, the predicted HRR profiles change based on the ventilation configuration, whereas the profiles from the fuel load, HRRPUA, and Duggan method are unchanged for different ventilation configurations. The peak HRR predicted by the heat of gasification model is 10,000 kW (9,478 Btu/s) higher than the other simplified models in the fourth ventilation configuration due to higher post-flashover gas temperatures with ventilation in the range $10 < OF < 20$. Using the peak HRR predicted using the other simplified models for design could result in a non-conservative design for the most aggressive ventilation configurations.

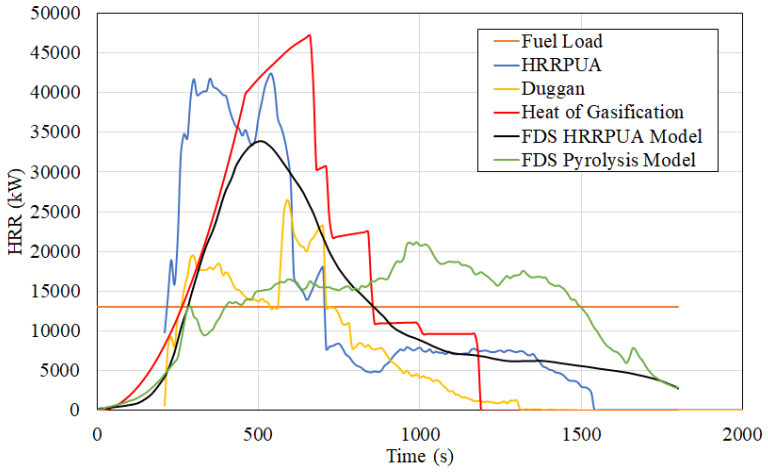

Figure 5-2. Rail car heat release rate predictions with Case 1 ventilation (two doors open) using several methods

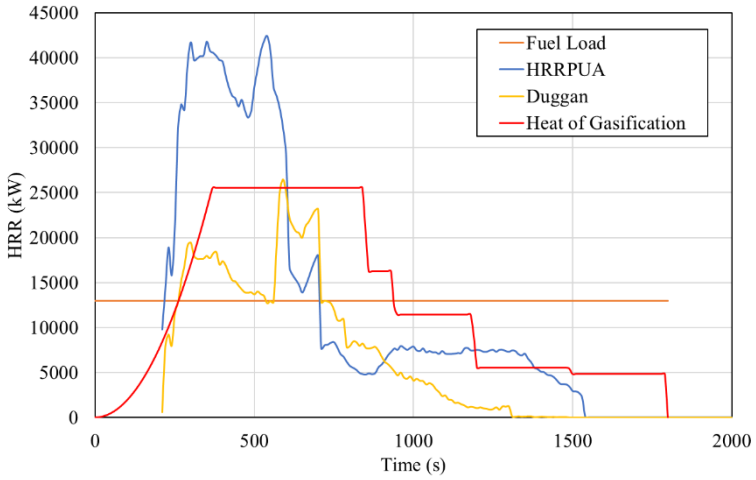

Figure 5-3. Rail car heat release rate predictions with Case 2 ventilation (one door open) using several methods

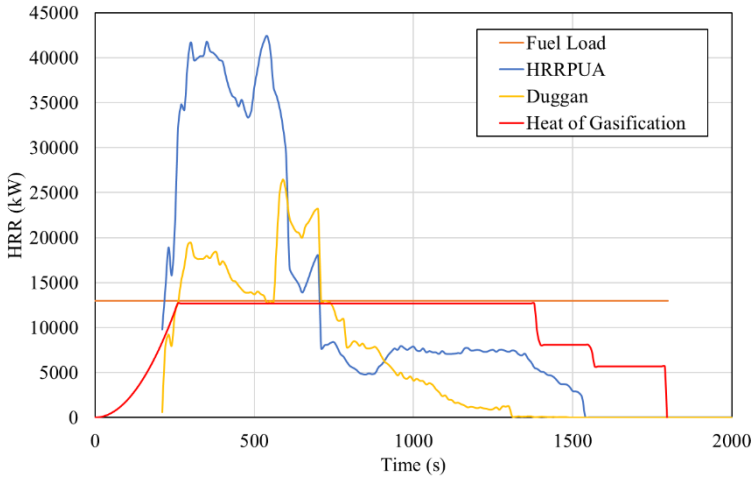

Figure 5-4. Rail car heat release rate predictions with Case 3 ventilation (one window open) using several methods

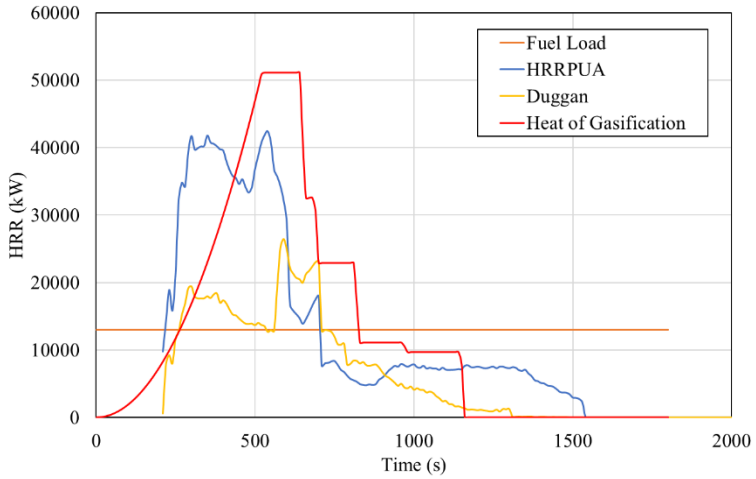

Figure 5-5. Rail car heat release rate predictions with Case 4 ventilation (four doors and six windows open) using several methods

5.5 Section Summary

This section presented a new simplified model to predict HRR in a fully-developed rail car fire based on heat of gasification. In the new model, gas temperatures are predicted using empirical relationships based on available ventilation instead of using a fire model. Overall, the peak HRR predicted were conservative relative to the FDS pyrolysis model, which is the expected HRR result. Since the gas temperatures vary based on the ventilation, the predicted HRR profile changes based on available ventilation, which is not possible with other simplified modeling approaches.

The new model is based on the following assumptions.

- All surfaces are initially ignited and experience the same exposure
- Exposure heat flux directly related to average gas temperature

- Failure times of any windows are known or can be estimated

The procedure to apply the new model to a new rail car consists of the following steps.

- Run cone calorimeter experiments for each rail car material at 50 kW/m^2 (4.4 Btu/s-ft^2) to determine $(\Delta H_c,\ \Delta H_g)$
- Calculate fuel loading for each material in rail car based on geometric design (E)
- Estimate window failure times based on design fire
- Calculate opening factor based on ventilation conditions (OF)
- Calculate gas temperature and net heat flux based on opening factor (T_g, q''_{net})
- Calculate HRR for each material based on heat flux and heat of gasification
- Calculate overall HRR by summing the HRR component for each material

The simplified model was determined to provide a conservative peak HRR compared with detailed simulations in FDS with the pyrolysis model. Additional comparison with detailed FDS simulations and experimental data is needed to further validate the new simplified model with other airflow conditions. In addition, methods to account for the spatial variation in the fire exposure inside of rail car need to be explored and incorporated into the simplified model.

6. Conclusion

This research effort focused on developing methods to quantify the overall HRR history of rail cars that includes all stages of the fire (growth, flashover, fully-developed and decay). This report provides the results of the initial development of scaling laws for use in developing cost effective experimental measurements of rail car HRR measurements as well as modeling approaches for predicting rail car HRR.

Scaling laws were successfully developed to predict the fire dynamics and material burning behavior in pre-flashover and fully-developed fires. Material burning was found to scale with HRRPUA, so dimensions should be scaled directly while thickness should remain constant to conserve energy. Froude modeling was found not to be sufficient to scale fully-developed compartment fire dynamics due to not being able to account for the effects of air flow on the compartment fire. Instead, scaling laws conserving opening factor should be used to scale the ventilation opening so that gas temperatures scale. The scaling laws were shown to be able to predict scaled compartment fire data from computer simulations using FDS and limited compartment fire data. Additional comparisons with data are required to more completely demonstrate their use.

A window failure model was developed using the FE model Abaqus and successfully used to predict window failure in available data. This model was used to explore scaling of windows, and it was shown that window thickness may need to be scaled based on the behavior of the full-scale window size. The complexity of the scaling resulted using the model itself to determine how smaller scale windows would respond and as a tool to design scaled windows that would have a response similar to full size windows.

The CFD model FDS was validated against fully-developed compartment fire data and then used to predict the HRR history of a rail car fire. A detailed pyrolysis model that predicts solid material burning was found to be necessary to accurately account for the spatial variations and low oxygen concentration effects on the thermal exposure. Model trends are similar to those measured for similar rail cars; however, a full validation was not possible due to insufficient data on the interior finish materials. Additional validation of the model with experimental data is needed to further quantify the uncertainty of the model with actual fires.

A simplified model to predict the HRR history was developed for use by designers and rail operators. This model uses empirical methods to predict the fire conditions based on the ventilation and interior surface area of the rail car. Material burning was predicted using a heat of gasification approach that allows for the burning rate to change based on the thermal exposure. This approach was found to account for the changes in ventilation of the rail car, which other simplified methods do not capture. Additional comparisons need to be made with FDS simulation results and experimental data to validate the model.

6.1 Future Work

The work included in this aspect of the research was based on the developing theoretical and computational methods to support predicting HRR histories of rail cars. To demonstrate these methods, it is recommended that a series of fire testing experiments be conducted. This would include simple room geometries as well as more complex geometries consistent with a rail car.

Experiments should be conducted at multiple scales to demonstrate the performance of scaling laws.

The initial fire testing experiments should be performed in a compartment consistent with the standard size NFPA 286 fire test room (2.44 m wide, 2.44 m high, 3.66 m deep [8.0 ft. x 8.0 ft. x 12.0 ft.]) with a single door opening (0.9 m wide and 2.0 m high [3 ft. wide and 6.6 ft. high]) as well as two scaled compartments (1:2 and 1:5). A second series of tests should then be conducted including a window (0.6 m wide and 0.6 m high [2 ft. wide and 2 ft. high]) on each of the two side walls of the compartment along with the door. Fires should include by a scaled gas burner both with and without combustible linings inside the compartment. The select test should also include polycarbonate windows to validate failure due to the fire exposure. Scaling laws developed in this research should be used to size the compartments, openings, burner, and combustible linings.

Validated scaling laws should then be used to scale a rail car (~1:5) including overall dimensions, opening dimensions, window for failure, and combustible interior finish. This will be done using an exemplar rail car design and materials tested and characterized in this research. Tests will then be performed varying the ventilation conditions to quantify the effects on HRR history.

An actual rail car should be acquired from industry and a large-scale test conducted to quantify the HRR history. Prior to large scale testing, the interior finish materials should be characterized using small-scale testing including cone calorimeter and TGA so that material properties for burning models can be determined. In addition, both scaled HRR testing and simulations should be performed prior to testing the full rail car to understand the behavior in support of designing the large-scale test.

Data collected in these experimental studies should be used to validate the detailed FDS model and simplified model developed in this work to predict HRR history. This validation will be used to further quantify the uncertainty of the predictive capabilities of these models. Currently, this is lacking in the industry and models are being used without being fully validated for rail car applications.

7. References

[1] Code of Federal Regulations, "Title 49 CFR § 238.103–Fire safety," vol. 79, no. 16., pp. 1–28, 2014.

[2] "NFPA 130 Standard for Fixed Guideway Transit and Passenger Rail Systems," National Fire Protection Association, Quincy, MA, 2017.

[3] Quintiere, J. G., "Scaling applications in fire research," *Fire Safety Journal*, *15*(1), pp. 3–29, 1989.

[4] Drysdale, D., "The Post-Flashover Compartment Fire," in *An Introduction to Fire Dynamics*, 2011, pp. 386–439.

[5] Li, Y. Z., and Ingason, H., *Correlations between different scales of metro carriage fire tests*. 2013.

[6] Bullen, M. L., "A Combined Overall and Surface Energy Balance for Fully-Developed Ventilation-Controlled Liquid Fuel Fires in Compartments," *Fire Technology*, *22*(3), pp. 257–259, 1976.

[7] Lee, B. T., "Quarter-scale room-fire tests of interior finishes," *Fire Materials: an International Journal*, *9*(4), pp. 185–191, 1985.

[8] Dingyi, H., "Evaluation of quarter-scale compartment fire modeling for constant and stepped heat inputs," *Fire Materials: an International Journal*, *11*(4), pp. 179–190, 1987.

[9] Bundy, M., et al., "NIST Technical Note 1483; Measurements of Heat and Combustion Products in Reduced-Scale Ventilation-Limited Compartment Fires NIST Technical Note 1483 Measurements of Heat and Combustion Products in Reduced-Scale Ventilation-Limited Compartment Fires," *U.S. Department Commerce*, no. 1483, p. 147, 2007.

[10] Strege, S., Lattimer, B., and Beyler, C., "Fire Induced Failure of Polycarbonate Windows in Railcars," 2005.

[11] Rippe, C., Lattimer, B., and Case, S., "Modeling Fire Induced Burnthrough Rupture of Marine Grade Aluminum Panels," in *Structures in Fire: Proceedings of the Ninth International Conference*, 2016, pp. 417–424.

[12] Rippe, C. M., "Burnthrough Modeling of Marine Grade Aluminum Alloy Structural Plates Exposed to Fire," Virginia Tech University, 2015.

[13] Larson, F. R., and Miller, J., "A Time-Temperature Relationship for Rupture and Creep Stresses," *Transactions of ASME*, vol. 74, pp. 765–771, 1952.

[14] Kachanov, L. M., "Rupture time under creep conditions," *International Journal of Fracture*, *97*(1–4), pp. 6–18, 1999.

[15] Rabotnov, I., *Creep Problems in Structural Members*. Amsterdam, Holland: North-Holland Publishing Company, 1969.

[16] Srivastava, V., Chester, S. A., Ames, N. M., and Anand, L., "A thermo-mechanically-coupled large-deformation theory for amorphous polymers in a temperature range which

spans their glass transition," *International Journal of Plasticity*, *26*(8), pp. 1138–1182, 2010.

[17] Caplan, E. S., and Brinson, H. F., "Nonlinear Viscoelastic Characterization of Polycarbonate," 1982.

[18] Chiam, B. H., "Numerical Simulation of a Metro Train Fire," Fire Engineering Research Report 05/1, Department of Civil Engineering, University of Canterbury, Christchurch, New Zealand, pp. 1–340, 2005.

[19] Lee, D. H., et al., "Estimations of heat release rate curve of railcar fire," *Journal of Mechanical Science Technology*, *27*(6), pp. 1665–1670, 2013.

[20] Chen, J., Yao, X., and Li, S., "Study on the Influence of Ventilation Condition on the Heat Release Rate of the CRH Passenger Rail Car," *Procedia Engineering*, vol. 62, pp. 1050–1056, 2013.

[21] Chen, J., Yao, X., Yan, G., and Guo, X., "Comparative Study on Heat Release Rate of High-speed Passenger Train Compartments," *Procedia Engineering.*, vol. 71, pp. 107–113, 2014.

[22] White, N., "Fire Development in Passenger Trains," *M.S. Thesis, Victoria University*, p. 323, 2010.

[23] Chen, J., and Yi, L., "Influence of Ventilation Status on Combustion Characteristics of Coach Fire," *Procedia Engineering*, vol. 52, pp. 42–47, 2013.

[24] Hadjisophocleous, G., Lee, D., and Park, W., "Full-scale experiments for heat release rate measurements of railcar fires," *Fifth International Symposium on Tunnel Safety and Security*, pp. 457–466, 2012.

[25] Lee, D. H., Park, W. H., and Jung, W. S., "Application Study of Burning Area-Based Summation Method for Fire Curve Estimation," *Structural Longevity*, *7*(3), pp. 161–166, 2012.

[26] Moinuddin, K. and Thomas, I., "An Experimental Study of Fire Development in Deep Enclosures and a New HRR-time-position Model for a Deep Enclosure Based on a Ventilation Factor," *Fire Materials: an International Journal*, vol. 33, pp. 157–185, 2009.

[27] Bullen, M. L. and Thomas, P. H., "Compartment fires with non-cellulosic fuels," *Symposium on Combustion*, 1979.

[28] Lautenberger, C., Rein, G., and Fernandez-Pello, C., "The application of a genetic algorithm to estimate material properties for fire modeling from bench-scale fire test data," *Fire Safety Journal*, *41*(3), pp. 204–214, 2006.

[29] Chaos, M., Khan, M. M., Krishnamoorthy, N., De Ris, J. L., and Dorofeev, S. B., "Evaluation of optimization schemes and determination of solid fuel properties for CFD fire models using bench-scale pyrolysis tests," *Proceedings of the Combustion Institute*, *33*(2), pp. 2599–2606, 2011.

[30] Kapahi, A. et al., "Evaluation of Rail Car Floor Fire Resistance Exposure and Test Article Scaling," 2018.

[31] American Society for Testing and Materials, “ASTM E1354-15a Standard Test Method for Heat and Visible Smoke Release Rates for Materials and Products Using an Oxygen Consumption Calorimeter,” West Conshohocken, PA, 2016.

Appendix A. Cone Calorimeter Validation for Rail Car Materials

The optimized material properties of the rail car material were validated in a 50 kW/m^2 FDS cone calorimeter simulation against the experimental data. The figures below show the results of this validation process.

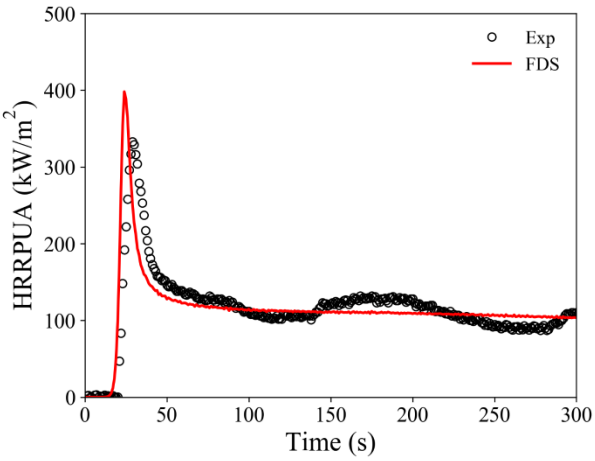

Figure A - 1. Sample 2 cone calorimeter validation results

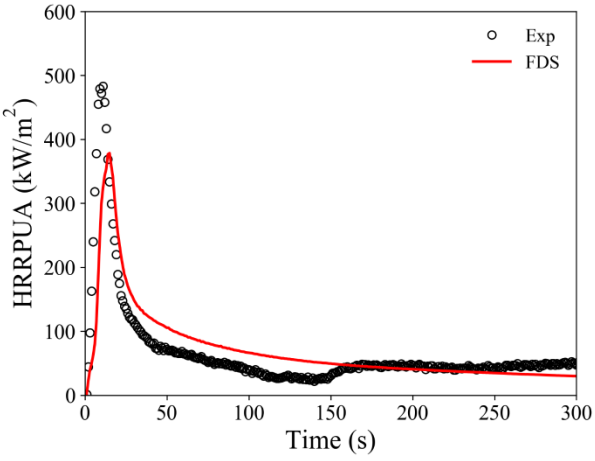

Figure A - 2. Sample 3 cone calorimeter validation results

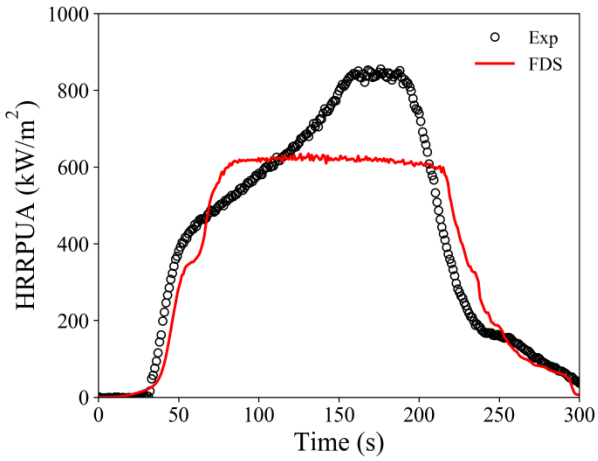

Figure A - 3. Sample 4 cone calorimeter validation results

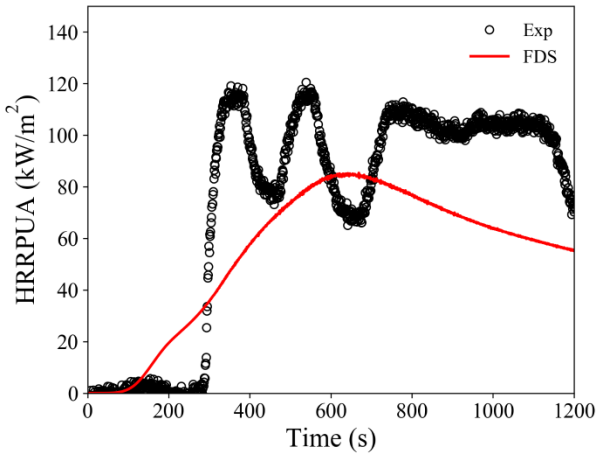

Figure A - 4. Sample 6 cone calorimeter validation results

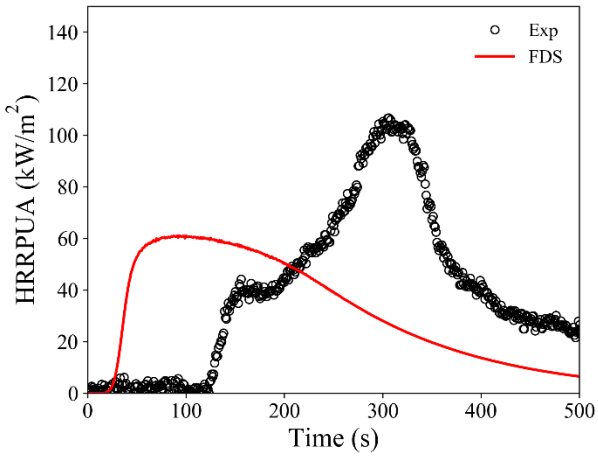

Figure A - 5. Sample 7 cone calorimeter validation results

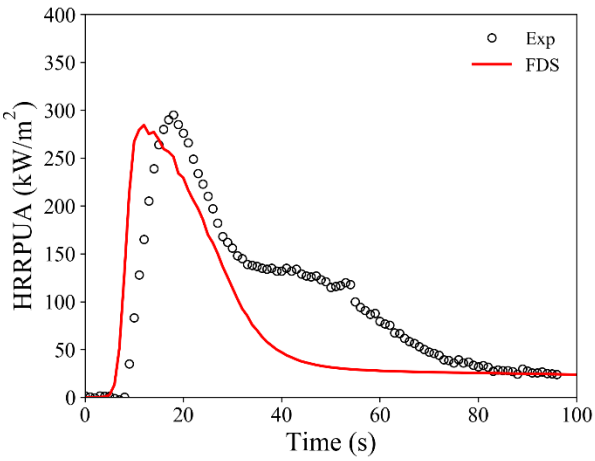

Figure A - 6. Sample 8 cone calorimeter validation results

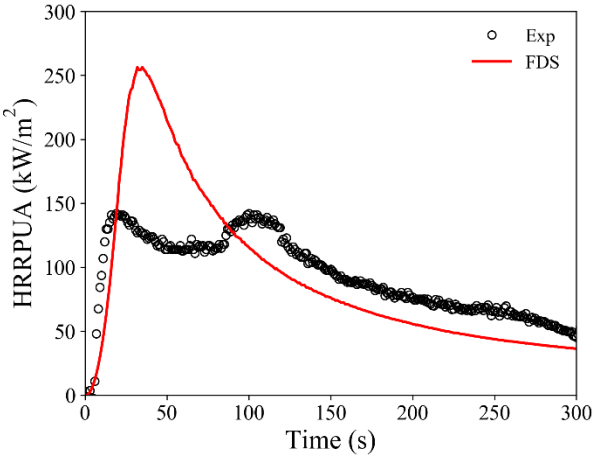

Figure A - 7. Sample 9 cone calorimeter validation results

Table A - 1 lists the optimized material properties below.

Table A - 1. Optimized material properties for Sample 1

Properties	Component 1	Component 2	Component 3	Char
A	3.42E+03	1E+18	2080000	
C_0	0.508156411	0.42513423	0.066709359	0
$C_{p,a}$	481.3607542	89.19997233	2125.785019	1508.646261
$C_{p,b}$	0.139646712	1.508653138	3.603458643	5.773442356
E	9.77E+04	304000	105000	
H_p	5579428.403	358770.7623	6889955.111	
K	424099.7889	748553.1298	570510.6702	566054.9412
ξ	7.50E-14	0.751730981	6.40432E-13	
ε	0.888205343	0.869784148	0.889042498	0.93474218
k_a	0.425799709	0.14359782	0.182801795	0.215570659
k_b	0.005775021	0.02123241	0.015532325	0.015786894
n	2.43E-15	2.705604735	0.9264385	
q''_{Ign}	12.64639846			
ρ	1314	1314	1314	683

Table A - 2. Optimized material properties for Sample 2

Properties	Component 1	Component 2	Component 3	Char
A	3.98E+08	2.08E+12	2.27E+21	
C_0	0.298090462	0.418756019	0.283153518	0
$C_{p,a}$	10.42605149	403.3896354	1203.760603	85.60639656
$C_{p,b}$	0.798773253	0.089402383	0.00143019	5.11767128
E	1.36E+05	148000	151000	
H_p	4722940.566	5809347.816	10066.84785	
K	814740.3134	272289.2583	572981.9862	190539.9387
ξ	0.240452125	0.000928094	0.566080043	
ε	0.94986624	0.949973187	0.907119381	0.986496894
k_a	0.138889867	0.401843876	0.643116938	0.001018235
k_b	0.01284438	0.036323591	0.028466059	0.001290582
n	0.37404579	4.067204252	14.51471543	
q''_{Ign}	24.99964019			
ρ	630	630	630	178

Table A - 3. Optimized material properties for Sample 3

Properties	Component 1	Component 2	Component 3	Char
A	1.00E+25	3.3E+14	1.32E+21	
C_0	0.211889891	0.418048058	0.370062051	0
$C_{p,a}$	1510.64009	15.02922796	631.1913309	2753.431901
$C_{p,b}$	3.386412154	0.029495902	0.016658286	5.636824802
E	9.43E+04	186000	206000	
H_p	35807.78493	9796831.038	32019.91151	
K	519885.7823	489199.3154	595289.8506	573499.2529
ξ	0.832676698	1.08196E-13	1.11379E-13	
ε	0.872659518	0.910375442	0.909607068	0.931363747
k_a	0.252310424	0.315184444	0.272546737	0.179514188
k_b	8.64E-05	0.013026789	0.000335222	0.000171048
n	20.29794614	1.626653118	8.428951668	
q''_{Ign}	14.88639074			
ρ	139.6	139.6	139.6	30

Table A - 4. Optimized material properties for Sample 4

Properties	Component 1	Component 2	Component 3
A	9.72E+10	372000000	60000000000
C_0	0.94642152	0.021351161	0.032227319
$C_{p,a}$	556.7702508	1945.973212	1698.613734
$C_{p,b}$	1.137727838	4.74854699	4.964078157
E	1.61E+05	38800	147000
H_p	2180001.671	5039165.462	3972806.621
K	500319.2403	499235.7782	548048.5985
ξ	0	0	0
ε	0.886952508	0.793359462	0.771710677
k_a	0.240318686	0.246396216	0.24267413
k_b	0.010862799	0.010551548	0.015711998
n	1.019407859	4.92299577	0.432326166
q''_{Ign}	30.65710314		
ρ	1178	1178	1178

Table A - 5. Optimized material properties for Sample 5

Properties	Component 1	Component 2	Component 3	Char
A	8.71E+15	13400	22500000	
C_0	0.087700892	0.050037192	0.862261916	0
$C_{p,a}$	2618.069986	2171.263178	168.1399178	2448.307297
$C_{p,b}$	4.562174095	0.580112865	0.002677129	8.475357135
E	2.48E+05	88000	147000	
H_p	9912522.468	3629046.064	3451929.241	
K	529269.4148	258047.5863	571258.5904	300743.8008
ξ	0.002330219	0.163261339	0.409588413	
ε	0.850237257	0.832590666	0.938350187	0.903777148
k_a	0.010799023	0.507030594	0.329371122	0.070744233
k_b	0.002602308	0.0245726	3.89686E-06	0.000492595
n	3.135998083	0.569525148	0.100000112	
q''_{Ign}	26.35200139			
ρ	1320	1320	1320	446

Table A - 6. Optimized material properties for Sample 6

Properties	Component 1	Component 2	Component 3	Char
A	2.45E+10	4.9E+16	9.7E+17	
C_0	0.28090347	0.298257314	0.420839216	0
$C_{p,a}$	10.87892288	2694.830591	326.1263652	584.9972109
$C_{p,b}$	5.776422666	0.312294238	5.940300809	2.810355057
E	1.59E+05	145000	204000	
H_p	1193046.238	3948602.48	131296.4922	
K	679204.0208	717781.8548	536131.4273	574818.5106
ξ	0.013845434	0.74664639	0.606514324	
ε	0.873610845	0.840635685	0.946644831	0.907949546
k_a	0.030385033	0.507166485	0.913271802	0.058283074
k_b	1.28E-05	3.50193E-06	0.000870998	1.74727E-05
n	1.170244196	6.962016961	5.301481518	
q''_{Ign}	29.07270057			
ρ	1600	1600	1600	800

Table A - 7. Optimized material properties for Sample 7

Properties	Component 1	Component 2	Component 3	Char
A	3.16E+15	3.54E+17	3.79E+17	
C_0	0.235554382	0.224749316	0.539696302	0
$C_{p,a}$	3135.075573	100.0128732	979.7898772	100.0076274
$C_{p,b}$	3.443870209	0.001027383	0.003028606	0.001009579
E	2.32E+05	694000	98800	
H_p	5868932.149	4652252.822	557849.0115	
K	589660.8115	610854.2276	372363.2426	391863.2166
ξ	0.457035008	0.393828068	0.785260009	
ε	0.889826195	0.901407389	0.882192821	0.953406323
k_a	0.358844567	0.168124078	0.414432181	0.115446586
k_b	0.017135879	0.01646643	0.014085068	0.016754083
n	4.4715657	5.481930639	30	
q''_{Ign}	49.99843976			
ρ	1846	1846	1846	1560

Table A - 8. Optimized material properties for Sample 8

Properties	Component 1	Component 2	Component 3	Char
A	1.08E+10	6710000000	2.75E+11	
C_0	0.610662347	0.083644242	0.305693411	0
$C_{p,a}$	10.08325799	1588.859367	10.12996285	3998.560446
$C_{p,b}$	0.001656386	7.030306575	3.822303287	9.985933275
E	1.22E+05	11600	172000	
H_p	1346343.479	9999963.517	9975700.311	
K	859863.4393	368084.4024	262697.9026	752178.5107
ξ	0.223770626	0.000386477	0.211168865	
ε	0.923558949	0.83323123	0.800913784	0.900008747
k_a	0.346886877	0.33613298	0.010032676	0.092111829
k_b	0.025299406	0.008285994	0.00194946	0.017636032
n	2.056460829	12.05408277	2.280097683	
q''_{Ign}	10.91213796			
ρ	1500	1500	1500	767

Table A - 9. Optimized material properties for Sample 9

Properties	Component 1	Component 2	Component 3	Char
A	1.00E+18	10000	119000000	
C_0	0.859241225	0.051225396	0.089533379	0
$C_{p,a}$	10.20126938	3718.377931	901.3259831	2551.956829
$C_{p,b}$	0.001643532	1.866857372	7.016227196	5.986037733
E	3.37E+05	38900	147000	
H_p	3236959.271	151270.696	5542870.408	
K	158650.8526	863583.5651	618706.9846	379986.0186
ξ	0.608444137	1.32295E-05	0.000116782	
ε	0.849891669	0.910620075	0.874242166	0.950827729
k_a	0.857403953	0.560155244	0.584107881	0.001907103
k_b	0.000293457	0.011470812	0.007694778	1.04328E-06
n	4.391705681	3.003303861	1.623441798	
q''_{Ign}	33.35126511			
ρ	100	100	100	71

Abbreviations and Acronyms

ACRONYM	EXPLANATION
ASTM	American Society of Testing Materials
CFD	Computational Fluid Dynamics
CFR	Code of Federal Regulations
DOT	Department of Transportation
EN	European Norm
FDS	Fire Dynamics Simulator
FE	Finite Element
FRA	Federal Railroad Administration
HRR	Heat Release Rate
HRRPUA	Heat Release Rate per Unit Area
ISO	International Standards Organization
IR	Infrared
LMP	Larson Miller Parameter
MLR	Mass Loss Rate
NFPA	National Fire Protection Association
NIST	National Institute of Standards and Technology
OF	Opening Factor
PMMA	Polymethylmethacrylate (plastic)
SCE	Shuffle Complex Evolution
SFPE	Society of Fire Protection Engineers
TGA	Thermogravimetric Analyzer
Volpe	Volpe National Transportation Systems Center